UiT
THE ARCTIC
UNIVERSITY
OF NORWAY

Faculty of Science and Technology
Department of Physics and Technology

SAR imaging and detection of partially coherent targets

—

Stein-Kato Lindberg

EOM-3901 Master's thesis in energy, climate and environment - June 2018

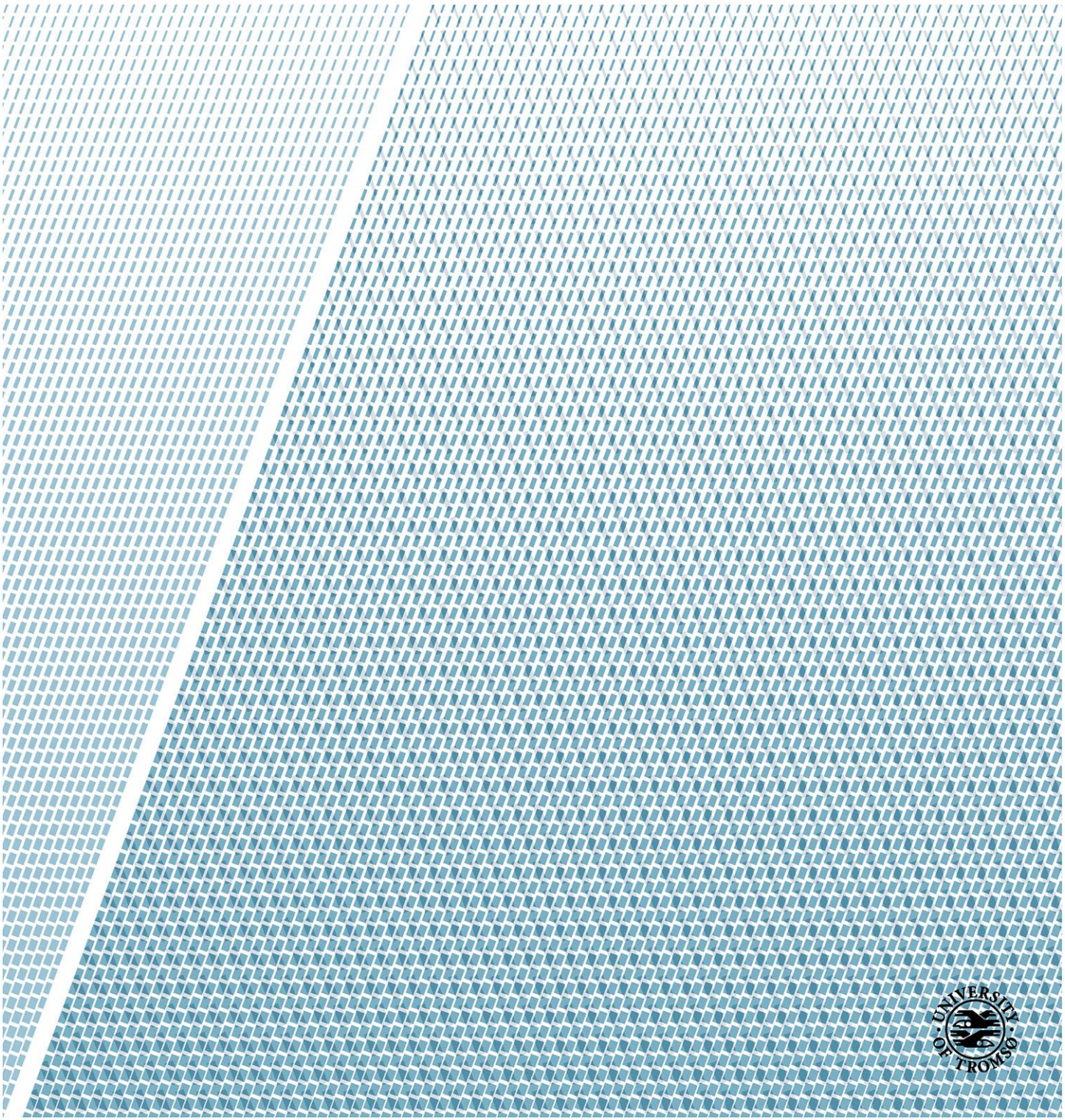

Abbreviations

FM Frequency Modulation

FWHP Full Width Half Power

IRW Impulse Response Width

NRCS Normalized Radar Cross Section

PRF Pulse Repetition Frequency

RAR Real Aperture Radar

RCM Range Cell Migration

RCMC Range Cell Migration Correction

RCS Radar Cross Section

SAR Synthetic Aperture Radar

TBP Time Bandwidth Product

Nomenclature

B_D Doppler bandwidth

β_a Radar azimuth beamwidth

$*$ Convolution

δ_a Azimuth resolution

δ_r range resolution

η Azimuth time

$\mathcal{F}$ Fourier transform

f_D Doppler frequency

f_s Sampling frequency

γ SAR processor coherence function

h (Matched) filter or impulse response

K_a Azimuth Doppler FM rate of change

K_r Range chirp FM rate of change

λ Radar wavelength

L_a Antenna length in azimuth direction

l_c Coherence length

n Additive receiver noise

P_r Power received at sensor

Q Quadratic filter

R_0 Distance of closest approach to target

ρ Autocorrelation function or charge distribution

σ Radar cross section

σ^0 radar backscattering coefficient

T_a Azimuth exposure time

τ Range time or autocorrelation lags

T_r SAR pulse duration

τ_c Coherence time

T_s Sampling period

V_g Speed of antenna footprint along ground

V_r Speed of antenna footprint under rectilinear approximation

V_s Speed of radar platform

w Azimuth Doppler prefilter

w_a Antenna pattern (azimuth dimension)

w_r Antenna pattern (range dimension)

Abstract

A synthetic aperture radar (SAR) achieves a high azimuth resolution by illuminating targets with multiple pulses and using the Doppler history to synthesize a large antenna. When combining the pulses, it is normally assumed that the targets are stationary, and that their reflectivity is independent of time. The topic of this thesis is the processing of SAR images where the the targets have a time-dependent reflectivity. One can imagine, for instance, a ship rolling in a rough sea. One possible way of processing such targets is described by Raney (1969a, 1980a, 1980b, 1981a). The goal of this thesis is to provide a well structured introduction into Raney's formalism on partially coherent targets, and to investigate a focusing strategy for scenes where the targets have different coherence times. The image formation processes of a synthetic aperture radar is thoroughly discussed, and a one-dimensional model of the azimuth dimension is introduced. Raney's formalism is compared to this model and found to be formally correct. A partially coherent point target is simulated, and Raney's formalism is tested for the purpose of target detection in the presence of scene partial coherence. It is shown that the whole system, including partial coherence in both scene and processor, behaves as a Gaussian low-pass filter weighted by the scene autocorrelation function and the processor coherence function.

Contents

List of Figures

List of Tables

Chapter 1

Introduction

The topic of this thesis is the processing of synthetic aperture radar (SAR) images where the scene consists of a point target with a time-varying reflectivity. SAR systems, being coherent imaging systems, generally assume that all targets are stationary when the return signals are combined into a single image (Vachon, 1983, ch. 2). While there exists methods for dealing with a moving target (Raney, 1971), a stochastic-time variation in a stationary target presents an entirely different challenge.

1.1 Objectives

The aim of this study is to investigate whether it is possible to process partially coherent targets in a way that facilitates target detection despite the partially coherent nature of the return signals. This investigation shall be based on Raney (1969a, 1980a, 1980b, 1981a) (henceforth collectively referred to as Raney's articles), who proposes the introduction of partial coherence in the SAR processor as a way of enhancing SAR images of partially coherent targets. This approach is formulated in continuous azimuth time in one dimension.

Central to this method is the theory of quadratic filters, which allows the use of the autocorrelation function of the the target's reflectivity variation to be exploited. This

in turn can be defined based on the target's coherence time, which is the only statistic required to implement this method of processing. The estimation of this statistic is beyond the scope of this study as it is not possible in general to obtain neither the coherence time not the autocorrelation function from SAR data (Raney, 1980b, p. 786). However, there exist methods of measuring coherence times for e.g. ocean waves (Carande, 1994; Shemer & Marom, 1993). In simulating partially coherent processing it shall therefore be assumed that a rough estimate of the coherence time is available.

An important motivation for the work by Raney on this topic is the description of how a SAR system interacts with azimuthal travelling ocean waves during imaging (Raney, 1980b, p. 784). This seems to have been a controversy at the time when these articles were published (Raney, 1981b; Alpers & Rufenach, 1979) with competing models still being in existence at least a decade afterwards (Kasilingam & Shemdin, 1990).

Raney's formalism shall be developed one step further by modifying the choice of quadratic filter in order to investigate the processing of scenes which contain targets with different correlation times.

1.2 Structure of the thesis

The starting point of this thesis is the theory of electromagnetic waves and radiation, which are the physical phenomena upon which a SAR system depends in order to function. This is covered in chapter 2.

Next, chapter 3 covers a small selection of topics in signal processing which are relevant to SAR processing, followed by a chapter devoted to the principles of radar systems in general.

This is followed by a thorough review of the theory of SAR systems in chapter 5 with a particular emphasis on the impulse response and resolution properties. The decoupling of the impulse response into its range and azimuth components is central to the theory of Raney, and shall be carried over to subsequent chapters.

Chapter 6 then proceeds with a unified presentation of quadratic filter theory, a neat way of formulating a non-linear system as a linear one, which allows all the well-known results of such systems to be exploited.

Partial coherence is the topic of chapter 7, which finishes the presentation of Raney's formalism and offers an evaluation of its validity in terms of the topics covered in previous chapters.

The final part of this thesis is reserved for simulating a simple one-dimensional SAR-system. Chapter 8 deals with simulating a point target in order to study the basic properties of the proposed method. Finally chapter 9 takes this one step further and presents a simulation of a point target embedded in a distributed scene, and a novel approach for processing such scenes is put to the test.

Chapter 2

Electromagnetic waves

This chapter gives a brief overview of electrodynamics relevant for remote sensing, starting with Maxwell's equations. From these the three-dimensional wave equation is rederived, and the finally a proof of Jefimenko's equations is sketched. The aim is to explain how the electric field is inversely proportional to the separation distance between source and observer, which shall subsequently be used to define the directivity and gain of a radar antenna.

2.1 Maxwell's equations

The study of electromagnetism is at its most fundamental level concerned with how a collection of charges, possibly undergoing some motion, affects another collection of charges at a different location. The classical theory describes the interaction between these charges by means of electric and magnetic fields which mediate the forces exchanged back and forth. In the static case these fields exist due to the presence of charges, while an accelerating charge causes a part of the field to detach itself from the charge and carry off energy, momentum and angular momentum at the speed of light. This is referred to as electromagnetic radiation and motivates the study of the fields themselves independent of the charges that produce them (Griffiths, 2013, p. xvi-xvii).

The theory of classical electrodynamics is contained in Maxwell's equations:

$$\nabla \cdot \mathbf{E} = \frac{1}{\epsilon_0}\rho \qquad \text{(Gauss's law)} \tag{2.1}$$

$$\nabla \cdot \mathbf{B} = 0 \qquad \text{(no name)} \tag{2.2}$$

$$\nabla \times \mathbf{E} = -\frac{\partial \mathbf{B}}{\partial t} \qquad \text{(Faraday's law)} \tag{2.3}$$

$$\nabla \times \mathbf{B} = \mu_0 \mathbf{J} + \mu_0 \epsilon_0 \frac{\partial \mathbf{E}}{\partial t} \qquad \text{(Ampère's law with Maxwell's correction)} \tag{2.4}$$

along with the force law, which describes the force $\mathbf{F}$ experienced by a charge q due to fields $\mathbf{E}$ and $\mathbf{B}$:

$$\mathbf{F} = q\left(\mathbf{E} + \mathbf{v} \times \mathbf{B}\right) \tag{2.5}$$

and suitable boundary conditions (Griffiths, 2013, ch. 7). $\mathbf{E}$ and $\mathbf{B}$ denote the electric and magnetic fields, and ρ and $\mathbf{J}$ represent charge and current densities. ϵ_0 and μ_0 are the permittivity and permeability of free space, with values:

$$\epsilon_0 = 8.85 \cdot 10^{-12}\,\mathrm{C^2 N m^{-2}} \tag{2.6}$$

$$\mu_0 = 4\pi \cdot 10^{-7}\,\mathrm{N A^{-2}} \tag{2.7}$$

Equation 2.5 describes the force applied to a charge q moving through the fields with velocity $\mathbf{v}$.

In free space, where there are no charges or currents, Maxwell's equations reduce to:

$$\nabla \cdot \mathbf{E} = 0 \tag{2.8}$$

$$\nabla \cdot \mathbf{B} = 0 \tag{2.9}$$

$$\nabla \times \mathbf{E} = -\frac{\partial \mathbf{B}}{\partial t} \tag{2.10}$$

$$\nabla \times \mathbf{B} = \mu_0 \epsilon_0 \frac{\partial \mathbf{E}}{\partial t} \tag{2.11}$$

Taking the curl of equation 2.10 and 2.11:

$$\nabla \times (\nabla \times \mathbf{E}) = \nabla(\nabla \cdot \mathbf{E}) - \nabla^2 \mathbf{E} = \nabla \times \left(-\frac{\partial \mathbf{B}}{\partial t} \right) \tag{2.12}$$

$$\nabla \times (\nabla \times \mathbf{B}) = \nabla(\nabla \cdot \mathbf{B}) - \nabla^2 \mathbf{B} = \nabla \times \left(\mu_0 \epsilon_0 \frac{\partial \mathbf{E}}{\partial t} \right) \tag{2.13}$$

and using equation 2.8 and 2.9:

$$\nabla^2 \mathbf{E} = -\nabla \times \left(-\frac{\partial \mathbf{B}}{\partial t} \right) = \frac{\partial}{\partial t}(\nabla \times \mathbf{B}) = \mu_0 \epsilon_0 \frac{\partial^2 \mathbf{E}}{\partial t^2} \tag{2.14}$$

$$\nabla^2 \mathbf{B} = -\nabla \times \left(\mu_0 \epsilon_0 \frac{\partial \mathbf{E}}{\partial t} \right) = -\mu_0 \epsilon_0 \frac{\partial}{\partial t}(\nabla \times \mathbf{E}) = \mu_0 \epsilon_0 \frac{\partial^2 \mathbf{B}}{\partial t^2} \tag{2.15}$$

Hence each Cartesian component of the fields satisfies the three-dimensional wave equation:

$$\nabla^2 f = \frac{1}{v^2} \frac{\partial^2 f}{\partial t^2} \tag{2.16}$$

with a propagation speed v given by:

$$v = \frac{1}{\sqrt{\epsilon_0 \mu_0}} \tag{2.17}$$

which turns out to be equal to the speed of light in vacuum. This important result underpins the classical theory of light as electromagnetic waves (Griffiths, 2013, ch. 9.1). It can further be show that for monochromatic plane waves, the electric and magnetic fields are mutually perpendicular, in phase and proportional (Griffiths, 2013, p. 396).

2.2 Radiation

The energy transported by the electric and magnetic fields, per unit time per unit area, is given by the Poynting vector $\mathbf{S}$, which is related to the fields by:

$$\mathbf{S} = \frac{1}{\mu_0}(\mathbf{E} \times \mathbf{B}) \tag{2.18}$$

The energy crossing an infinitesimal surface $d\mathbf{a}$ per unit time (the energy flux) is equal to $\mathbf{S} \cdot d\mathbf{a}$. Hence $\mathbf{S}$ is referred to as the energy flux density (Griffiths, 2013, ch. 8.1).

As mentioned, the acceleration of a charge causes energy to be transported away by the fields. The transportation of energy to infinity is referred to as radiation. This term is often used in the broader sense of any field with a non-zero Poynting vector, but shall here be restricted to the former sense of the word.

Consider a localized radiating source at the centre of a sphere with radius r. The power $P(r,t)$ passing through this sphere is:

$$P(r,t) = \oint \mathbf{S} \cdot d\mathbf{a} \tag{2.19}$$

The energy arriving at the sphere at a time t depends on the retarded time $t_0 = t - \frac{r}{c}$ since electromagnetic waves travel at the speed of light. Letting $r \to \infty$, the radiated power is then:

$$P_{rad}(t_0) = \lim_{r\to\infty} P\left(r, t_0 + \frac{r}{c}\right) \tag{2.20}$$

(Griffiths, 2013, ch. 11.1). The differential $d\mathbf{a}$ is equal to $r^2 \sin\varphi d\theta d\varphi$, where θ and φ are the azimuth and zenith angles respectively (Weisstein, n.d.). Hence the only parts of the fields which reach to infinity are the ones with a Poynting vector that decreases by no more than r^{-2} at large r. If the fields go like r^{-1}, then the r^{-2} factor in the Poynting vector cancels out the r^2 factor in $d\mathbf{a}$, rendering the whole expression independent of propagation distance.

In the static case the electric field is given by Coulomb's law:

$$\mathbf{E}(\mathbf{r}) = \frac{1}{4\pi\epsilon_0} \int \frac{\rho(\mathbf{r}')}{\mathscr{r}^2} \hat{\boldsymbol{\mathscr{r}}}\, d\tau' \tag{2.21}$$

which describes the electric field at a point $\mathbf{r}$ in terms of the charge distribution ρ at a point $\mathbf{r}'$, with $\boldsymbol{\imath} = \mathbf{r} - \mathbf{r}'$, $\imath = \|\boldsymbol{\imath}\|$, $\hat{\boldsymbol{\imath}} = \frac{\boldsymbol{\imath}}{\imath}$, and $d\tau'$ being an infinitesimal volume element (Griffiths, 2013, p. 63).

The magnetic field is similarly given by the Biot-Savart law:

$$\mathbf{B}(\mathbf{r}) = \frac{\mu_0}{4\pi} \int \frac{\mathbf{I} \times \hat{\boldsymbol{\imath}}}{\imath^2} \, dl' = \frac{\mu_0}{4\pi} I \int \frac{d\mathbf{l}' \times \hat{\boldsymbol{\imath}}}{\imath^2} \tag{2.22}$$

where $\mathbf{I}$ denotes a steady current and dl' an infinitesimal line element (Griffiths, 2013, p. 224). Both these field go like $\imath^{-2}$, and hence produce no radiation.

The potentials of these fields are:

$$V(\mathbf{r}) = \frac{1}{4\pi\epsilon_0} \int \frac{\rho(\mathbf{r}')}{\imath} \, d\tau' \tag{2.23}$$

$$\mathbf{A}(\mathbf{r}) = \frac{\mu_0}{4\pi} \int \frac{\mathbf{J}(\mathbf{r}')}{\imath} \, d\tau' \tag{2.24}$$

respectively. It can be shown that the generalization for non-static sources is simply the same expressions evaluated at the retarded time $t_r = t - \frac{\imath}{c}$:

$$V(\mathbf{r}) = \frac{1}{4\pi\epsilon_0} \int \frac{\rho(\mathbf{r}', t_r)}{\imath} \, d\tau' \tag{2.25}$$

$$\mathbf{A}(\mathbf{r}) = \frac{\mu_0}{4\pi} \int \frac{\mathbf{J}(\mathbf{r}', t_r)}{\imath} \, d\tau' \tag{2.26}$$

The corresponding fields are then given by the relations:

$$\mathbf{E} = -\nabla V - \frac{\partial \mathbf{A}}{\partial t} \tag{2.27}$$

$$\mathbf{B} = \nabla \times \mathbf{A} \tag{2.28}$$

which yield Jefimenko's equations:

$$\mathbf{E}(\mathbf{r},t) = \frac{1}{4\pi\epsilon_0}\int\left(\frac{\rho(\mathbf{r}',t_r)}{\imath^2}\hat{\boldsymbol{\imath}} + \frac{\dot{\rho}(\mathbf{r}',t_r)}{c\imath} - \frac{\dot{\mathbf{J}}(\mathbf{r}',t_r)}{c^2\imath}\right)d\tau' \tag{2.29}$$

$$\mathbf{B}(\mathbf{r},t) = \frac{\mu_0}{4\pi}\int\left(\frac{\mathbf{J}(\mathbf{r}',t_r)}{\imath^2} + \frac{\dot{\mathbf{J}}(\mathbf{r}',t_r)}{c\imath}\right)\times\hat{\boldsymbol{\imath}}\,d\tau' \tag{2.30}$$

where $\dot{\rho}$ and $\dot{\mathbf{J}}$ denote time derivatives. These expressions do indeed contain terms that decrease at a rate $\imath^{-1}$, and the radiation for any ρ and $\mathbf{J}$ can be determined by picking out these terms (Griffiths, 2013, p. 444-450).

Chapter 3

Signal processing

The electromagnetic wave equation derived in the previous chapter lays the foundation for classical electrodynamics where electromagnetic radiation is considered as waves. Such waves can be represented as sinusoids, and this chapter treats the processing of sinusoidal signals, and linear frequency modulated (FM) signals in particular. It shall be discussed in the following chapter how such signals play an important role in SAR processing. Linear time-invariant systems shall also be discussed, as well as the Fourier transform, which offers an efficient way of implementing and analyzing such systems.

3.1 Linear FM signals

A sinusoidal signal $x(t)$ can be represented as a complex exponential:

$$x(t) = Ae^{i(\omega_0 t+\varphi)} \tag{3.1}$$

due to Euler's formula:

$$e^{ix} = \cos x + i \sin x \tag{3.2}$$

Here $i = \sqrt{(-1)}$ represents the imaginary unit. A complex exponential $e^{i\theta}$ is referred to as a phasor and represents a rotation in the complex plane by an angle θ

(McClellan, Schafer, & Yoder, 2003, p. 18-19).

If the angle of rotation is given by a function $\psi(t)$ instead of a constant angular frequency ω_0 and phase φ, then the instantaneous frequency is:

$$\omega(t) = \frac{d}{dt}\psi(t) \tag{3.3}$$

This frequency variation is referred to as frequency modulation. If $\psi(t)$ is a second-order polynomial in t, then the instantaneous frequency is a linear function of t. Such a linear FM signal is called a chirp (McClellan et al., 2003, p. 60-61).

3.2 Linear time-invariant systems

Consider a continuous-time system which maps an input $x(t)$ to an output $y(t)$:

$$x(t) \mapsto y(t) \tag{3.4}$$

Such a system is said to be time-invariant if:

$$x(t - t_0) \mapsto y(t - t_0) \tag{3.5}$$

That is, if the input is delayed by an amount of time t_0, then the output is delayed by the same amount of time.

Furthermore, suppose that two pairs of input and output signals for the same system are given by:

$$\begin{aligned} x_1(t) &\mapsto y_1(t) \\ x_2(t) &\mapsto y_2(t) \end{aligned} \tag{3.6}$$

If a linear combination of the two input signals $x(t) = \alpha x_1(t) + \beta x_2(t)$ is used as a new input, then a linear system will produce the output:

$$\alpha x_1(t) + \beta x_2(t) \mapsto \alpha y_1(t) + \beta y_2(t) \tag{3.7}$$

A system for which linearity and time-invariance both hold is referred to as a linear time-invariant (LTI) system (McClellan et al., 2003, p. ch. 9).

One useful property of LTI systems is that they are fully characterized by their impulse response $h(t)$. This is obtained by feeding a unit impulse to the system and observe the output. Hence, if $\delta(t)$ is a unit impulse at $t = 0$, then it relates to the impulse response by:

$$\delta(t) \mapsto h(t) \tag{3.8}$$

The unit impulse response is more commonly referred to as the Dirac delta function, which is not an actual function, but rather a generalized function or distribution (Zauderer, 2006, ch. 7.2). It has the properties that it is zero everywhere except at the origin, and that:

$$\int_{-\infty}^{\infty} \delta(t)dt = 1 \tag{3.9}$$

It is perhaps more properly defined by the relation:

$$\int_{-\infty}^{\infty} f(t)\delta(t - t_0) = f(t_0) \tag{3.10}$$

for any given function $f(t)$.

If the impulse response of an LTI system is known, then it can be described by a convolution integral:

$$y(t) = \int_{-\infty}^{\infty} x(\tau)h(t - \tau)d\tau \tag{3.11}$$

which relates the output directly to the input through the impulse response. The convolution operation is usually represented by the symbol $*$. Equation 3.11 is then more compactly expressed as:

$$y(t) = x(t) * h(t) \tag{3.12}$$

Since the integral in equation 3.11 is an improper one, the question of existence arises.

A function $f(t)$ is said to be of class L_p if:

$$\int_{-\infty}^{\infty} |f(t)|^p < \infty \tag{3.13}$$

For two L_1 functions $f(t)$ and $h(t)$, the convolution theorem states that the integral:

$$g(t) = \int_{-\infty}^{\infty} f(t-\tau)h(\tau)d\tau \tag{3.14}$$

exists, although not necessarily for all values of t (Brown, 1963, p. 313-314).

3.3 The Fourier transform

A signal $x(t)$ is said to be periodic if $x(t+T_0) = x(t)$ for all values of t. The smallest value of T_0 which satisfies this equation is referred to as the fundamental period, and its inverse $f_0 = \frac{1}{T_0}$ is called the fundamental (cyclic) frequency. The cyclic frequency f is related to the angular frequency ω by $\omega = 2\pi f$.

The theory of Fourier series states that any periodic signal can be expressed as a weighted sum of sines and cosines with frequencies that are integer multiples of the fundamental frequency of the signal (McClellan et al., 2003, ch. 3). Expressing this by means of a complex exponential:

$$x(t) = \frac{1}{\sqrt{T_0}} \sum_{k=-\infty}^{\infty} a_k \, e^{i2\pi k f_0 t} = \sum_{k=-\infty}^{\infty} a_k v_k \tag{3.15}$$

for $k \in \mathbb{Z}$, where $v_k(t) \equiv \frac{1}{\sqrt{T_0}} e^{i2\pi f_0 kt}$ forms an orthonormal set[1] on $[-\frac{T_0}{2}, \frac{T_0}{2}]$ with the inner product:

$$\langle f, g \rangle \equiv \int_{-\frac{T_0}{2}}^{\frac{T_0}{2}} f(t) g^*(t)\, dt \tag{3.16}$$

Using Fourier's trick, apply the inner product with $v_l(t)$ to equation 3.15:

$$\langle x, v_l \rangle = \sum_{k=-\infty}^{\infty} a_k \langle v_k, v_l \rangle = a_k \tag{3.17}$$

due to the orthonormality property, which yields the formula:

$$a_k = \frac{1}{\sqrt{T_0}} \int_{-\frac{T_0}{2}}^{\frac{T_0}{2}} x(t) e^{-i2\pi k f_0 t}\, dt \tag{3.18}$$

(McClellan et al., 2003, p. 48-50). The set $\{f_k, a_k\}$ is referred to as the spectrum of the signal, with $f_k \equiv k f_0$ being the k^{th} harmonic of f_0.

This formalism can be extended to include non-periodic functions by letting $T_0 \to \infty$ (McClellan et al., 2003, p. 307-312). In this limit the set $\{k f_0\}$ becomes a continuous variable f due to the inverse relations between T_0 and f_0. Rewriting equation 3.15 to:

$$x(t) = \frac{1}{2\pi} \sum_{k=-\infty}^{\infty} \left(a_k \sqrt{T_0} \right) e^{i2\pi f t} \left(\frac{2\pi}{T_0} \right) \tag{3.19}$$

the factor $\frac{2\pi}{T_0}$ can be identified as an infinitesimal angular frequency element $d\omega$. This expression is then a Riemann sum, and the summation can be replaced by an integral:

$$x(t) = \frac{1}{2\pi} \int_{\infty}^{\infty} \left(a_k \sqrt{T_0} \right) e^{i\omega t}\, d\omega \tag{3.20}$$

[1]Two vectors f and g in an inner product space (i.e., a vector space with an inner product) are said to be orthogonal if $\langle f, g \rangle = 0$. The norm of a vector f can be expressed as $\|f\| = \sqrt{\langle f, f \rangle}$. If each vector in a set are orthogonal and has norm 1, then the set is said to be orthonormal (Anton & Rorres, 2011, ch. 6).

Hence:

$$a_k\sqrt{T_0} = \int_{-\infty}^{\infty} x(t)e^{-i\omega t}\,dt \equiv X(\omega) \tag{3.21}$$

is defined as the Fourier transform of $x(t)$, with the inverse transform being given by equation 3.20.[2]

The transform so far considered is referred to as the continous Fourier transform (CFT). In the case where $x(t)$ has been sampled, yielding a set $x[n]$ of N samples, the discrete time Fourier transform (DTFT) is applied instead. The sampling process can be represented as a multiplication with an impulse train:

$$x[n] = x(nT_s) = x(t)\sum_{n=-\infty}^{\infty}\delta(t-nT_s), n = 0, 1, ..., L-1 \tag{3.22}$$

where T_s is the sampling period. Substituting $x[n]$ for $x(t)$ in equation 3.21:

$$\begin{aligned} X(\omega) &= \int_{-\infty}^{\infty} x(t)\sum_{n=-\infty}^{\infty}\delta(t-nT_s)e^{-i\omega t}\,dt \\ &= \sum_{n=-\infty}^{\infty}\int_{-\infty}^{\infty} x(t)\delta(t-nT_s)e^{-i\omega t}\,dt \\ &= \sum_{n=0}^{L-1} x(nT_s)e^{-i\omega nT_s} \end{aligned} \tag{3.23}$$

In numerical calculations the Fourier transform is evaluated at a discrete set of N evenly spaced frequencies $\omega_k = \frac{2\pi k}{NT_s}$ for $k = 0, 1, ..., N-1$, the result of which is the discrete Fourier transform (DFT):

$$X[k] = \sum_{n=0}^{L-1} x[n]e^{-i\frac{2\pi kn}{N}}, \quad k = 0, 1, ..., N-1 \tag{3.24}$$

If $N = L$ there exists an exact inverse transform:

[2]Equation 3.20 can also be written as $x(t) = \frac{1}{\sqrt{2\pi}}\int_{\infty}^{\infty}\left(\frac{a_k\sqrt{T_0}}{\sqrt{2\pi}}\right)e^{i\omega t}\,d\omega$, in which case there is a factor $\frac{1}{\sqrt{2\pi}}$ in both the Fourier transform and the inverse Fourier transform. Some authors, e.g. Zauderer (2006), prefer this due to the symmetry it provides.

$$x[n] = \frac{1}{N}\sum_{k=0}^{N-1} X[k]e^{i\frac{2\pi kn}{N}}, \quad n = 0, 1, ..., N-1 \tag{3.25}$$

and efficient computer algorithms for performing the calculations, collectively referred to as the fast Fourier transform (FFT) (McClellan et al., 2003, ch. 13).

The extension to two variables is straightforward. The CFT for a continuous function $f(x, y)$ is:

$$F(\omega, \lambda) = \int_{-\infty}^{\infty}\int_{-\infty}^{\infty} f(x, y)e^{-i\omega x}e^{-i\lambda y}\, dx\, dy \tag{3.26}$$

$$f(x, y) = \int_{-\infty}^{\infty}\int_{-\infty}^{\infty} F(\omega, \lambda)e^{i\omega x}e^{i\lambda y}\, d\omega\, d\lambda \tag{3.27}$$

(Raney, 1969a). Similarly, for an $M \times N$ discrete sample, such as a digital image, the DFT is:

$$F[u, v] = \sum_{x=0}^{M-1}\sum_{y=0}^{N-1} f[x, y]e^{-i\frac{ux}{M}}e^{-i\frac{vy}{N}} \tag{3.28}$$

$$f[x, y] = \frac{1}{MN}\sum_{u=0}^{M-1}\sum_{v=0}^{N-1} F[u, v]e^{i\frac{ux}{M}}e^{i\frac{vy}{N}} \tag{3.29}$$

(Gonzales & Woods, 2010, p. 257-258). The Fourier transform is useful for signal processing purposes due to the way operations on signals transform, e.g. the convolution of two signals in the time domain becomes multiplication of their respective Fourier transforms in the frequency domain. Hence convolution and multiplication forms a Fourier transform pair:

$$x(t) * h(t) \leftrightarrow X(\omega)H(\omega) \tag{3.30}$$

(McClellan et al., 2003, p. 327-328). Filtering of large vectors or matrices can be performed more efficiently in the frequency domain. In order to obtain a correct result it is required that two time-limited signals be zero-padded up to at least the sum of

their lengths minus one (along each individual axis in the 2D case). Otherwise the resulting convolution will be circular, sometimes referred to as wrap-around errors (Gonzales & Woods, 2010, ch. 7).

The Fourier transform as an operation shall be denoted by $\mathcal{F}$, and the inverse Fourier transform by $\mathcal{F}^{-1}$.

Chapter 4

Radar

Having discussed electromagnetic waves, the present chapter builds upon this topic in order to explain the principle of radar systems. The inverse dependence of the electric field on the separation between source and observer shall be used in order to define the antenna directivity and gain. Then the radar equation is rederived, and finally the beamwidth of a linear antenna array is discussed. The latter shall prove useful in subsequent simulations.

4.1 Principles of radar systems

Radar (RAdio Detection And Ranging) systems work by transmitting pulses of electromagnetic radiation in the radio wave part of the spectrum, which are in the range of 3 MHz and 300 GHz (Kingsley & Quegan, 1992, chapter 1). Each pulse is timed by the radar clock and propagate at the speed of light. Once a pulse hit a target the energy in the pulse is scattered, and part of it is returned to the receiver. The range, i.e. distance to the target, is then given by:

$$R = \frac{c\tau_d}{2} \tag{4.1}$$

where R is range, $c \approx 3 \times 10^8$ ms^{-1} is the speed of light in vacuum[1] and τ_d is the signal propagation delay.

The properties of a radar antenna is described by the antenna pattern, which quantifies the antenna's ability to focus energy in a given direction. Let the transmitted electric field be given by:

$$\boldsymbol{E} = \frac{1}{r} e^{-ikr} \boldsymbol{F}(\boldsymbol{k}) \tag{4.2}$$

for some $\boldsymbol{F}(\boldsymbol{k})$, which is justified by results in section 2.2. The squared norm of $\boldsymbol{F}(\boldsymbol{k})$, which depends on the wave vector $\boldsymbol{k}$, is then the radiated energy distribution, and the antenna directivity is:

$$\boldsymbol{D}(\boldsymbol{k}) = \frac{4\pi \|\boldsymbol{F}(\hat{\boldsymbol{k}})\|^2}{\int_0^{4\pi} \|\boldsymbol{F}(\hat{\boldsymbol{k}})\|^2 d\Omega} \tag{4.3}$$

where $\hat{\boldsymbol{k}} = \frac{\boldsymbol{k}}{\|\boldsymbol{k}\|}$ and $d\Omega$ is a differential solid angle element. For a lossy antenna there is also an efficiency factor η, which defines the antenna gain:

$$G(\hat{\boldsymbol{k}}) = \eta D(\hat{\boldsymbol{k}}) \tag{4.4}$$

(Massonet & Souyris, 2008). For an isotropic antenna $\|\boldsymbol{F}(\hat{\boldsymbol{k}})\|^2$ is constant, and hence $D = 1$. If in addition the antenna is lossless, then $G = 1$ as well.

The ability to focus transmitted energy may also describe the sensitivity of the antenna to received energy. If reciprocity is assumed, then the antenna pattern describes both (Kingsley & Quegan, 1992, p. 7).

[1]The speed at which light travels depends on the index of refraction of the medium through which it is propagating. The refractive index of air is approximately 1, which justifies using the value of c in vacuum for Earth observation purposes.

4.2 The radar equation

An antenna radiating power isotropically with a peak power P_t gives rise to a power flux at a distance R:

$$\texttt{Power flux at distance R} = \frac{P_t}{4\pi R^2} \tag{4.5}$$

since $4\pi R^2$ is the area of a sphere with radius R (Kingsley & Quegan, 1992, p. 11-15). Given a non-isotropic antenna there is an additional gain factor G_t which modifies the amount of power concentrated towards the target, hence yielding a power flux at the target:

$$\texttt{Power flux at target} = \frac{G_t P_t}{4\pi R^2} \tag{4.6}$$

The amount of power re-radiated by the target is described by the target's radar cross section (RCS) σ, which is defined as *"the power re-radiated towards the radar per unit solid angle divided by the incident power flux/4π radians"* (Kingsley & Quegan, 1992, p. 12), and may depend on incidence angle, radar frequency, polarization, dielectric properties, roughness, time etc. This can be understood as the cross-section of an isotropic radiator re-radiating the same amount of power. Hence:

$$\texttt{Re-radiated power} = \frac{P_t G_t \sigma}{4\pi R^2} \tag{4.7}$$

The return trip adds another factor $4\pi R^2$ to the denominator, and the amount of power which the antenna sees is determined by the effective antenna area[2] A_e, which enters as a factor in the numerator, yielding an expression for the received power P_r:

$$P_r = \frac{P_t G_t \sigma A_e}{(4\pi R^2)^2} \tag{4.8}$$

[2]The effective area of an antenna is related to the actual by $A_e = \eta A$, where η is an efficiency factor. For parabolic dishes η is usually takes values between 0.4 and 0.9, while television antennas can have an effective area which is greater than their actual cross-section (Kingsley & Quegan, 1992, p. 9).

The gain of the receiving antenna can be expressed as a function of the effective area and radar wavelength:

$$G_r = \frac{4\pi A_e}{\lambda^2} \tag{4.9}$$

which may be substituted into the previous equation. Adding an efficiency factor L_s to take system loss into account yields the full radar equation:

$$P_r = \frac{P_t G_t G_r \sigma \lambda_s^2 L_s}{(4\pi)^3 R^4} \tag{4.10}$$

In the presence of an average noise power N the signal-to-noise ratio (SNR) can be useful since this is by definition:

$$SNR = \frac{P_r}{N} = \frac{P_t G_t G_r \sigma \lambda_s^2}{(4\pi)^3 R^4 N} \tag{4.11}$$

if the noise properties of the system are known.

4.3 Antenna beam width

Consider two point radiators separated by a distance d with a phase difference α. An observer in the far field oriented at an angle θ will then observe an additional phase difference due to the difference in path length from the two radiators, which is given by $d \sin\theta$. This phase difference is then the number of wavelengths in $d \sin\theta$ multiplied by 2π. This is illustrated in figure 4.1.

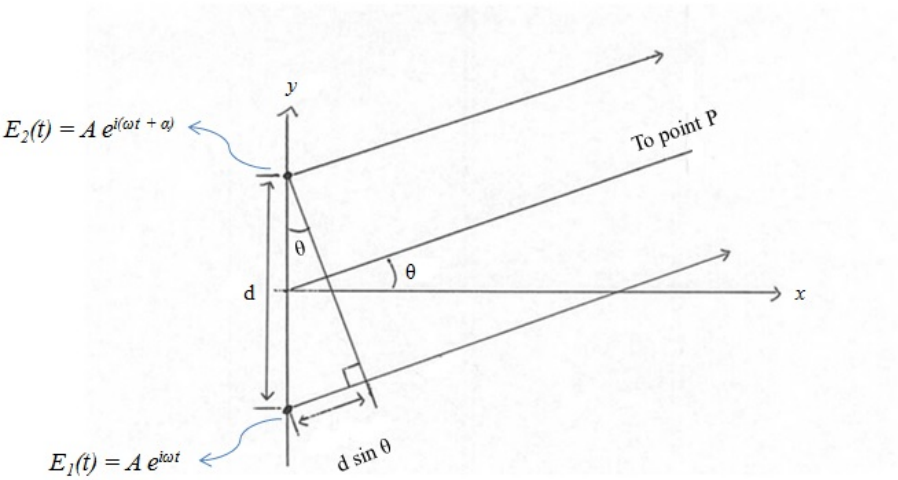

Figure 4.1: Geometry of two point radiators observed from an angle θ in the far field. Based on figure 29-10 in Feynman et al. (1963).

The observed phase difference is therefore:

$$\varphi_2 - \varphi_1 = \alpha + \frac{2\pi d \sin\theta}{\lambda} = \alpha + kd\sin\theta \tag{4.12}$$

where $k = \frac{2\pi}{\lambda}$ is the wave number (Feynman, Leighton, & Sands, 1963, p. 29-5).

Using this result, Elachi and van Zyl (2006, p. 222-225) derives an expression for the beam width of a linear array antenna as a function of radar wavelength and array length. The aim of this section is to explain the mysterious factor 0.886 which appears in a number of equations dealing with SAR systems, such as in Cumming and Wong (2005, ch. 4).

Given a linear array of N equally spaced radiators which are position a distance d apart, and which have the same amplitude and phase, the total far field is proportional to:

$$E(\theta) \propto e^{i\alpha} \sum_{n=1}^{N} e^{-inkd\sin\theta} \tag{4.13}$$

In the limit where N goes to infinity, this sum can be replaced with an integral:

$$E(\theta) \propto \int_{-\frac{D}{2}}^{\frac{D}{2}} e^{-ikx\sin\theta} dx \tag{4.14}$$

where it is assumed that the amplitude is uniform across the antenna (which has length D) and the phase is set to 0. Using the inverse Euler relation $\sin x = \frac{e^{ix}-e^{-ix}}{2i}$, his integral evaluates to:

$$E(\theta) \propto D\frac{\sin\left(\frac{kD\sin\theta}{2}\right)}{\frac{kD\sin\theta}{2}} \equiv D\,\mathrm{sinc}\left(\frac{kD\sin\theta}{2}\right) \tag{4.15}$$

In the discrete case, the nulls of $E(\theta)$ occur where the angles between the vectors $e^{-inkd\sin\theta}$ in the complex plane are evenly spaced. This implies that:

$$Nkd\sin\theta = 2m\pi \tag{4.16}$$

where m is an integer, and that the nulls are located at:

$$\theta = \sin^{-1}\left(\frac{2m\pi}{Nkd}\right) \tag{4.17}$$

In the continuous case nd is replaced by D. Noting that $k = \frac{2\pi}{\lambda}$:

$$D\sin\theta = m\lambda \tag{4.18}$$

with nulls at:

$$\theta = \sin^{-1}\frac{m\lambda}{D} \tag{4.19}$$

Setting $M = 1$, and if the wavelength is small compared to the antenna length, then, by the small angle approximation, the first null θ_0 is located at:

$$\theta_0 \approx \frac{\lambda}{D} \tag{4.20}$$

This is also a good approximation to the fulifthl width half-power (FWHP) beam width, which is given by:

$$\theta_{FWHP} \approx 0.886\frac{\lambda}{D} \tag{4.21}$$

The derivation of the FWHP beamwidth can be found in Appendix A.

Chapter 5

Synthetic aperture radar

The previous chapters have covered some basic topics of electromagnetic radiation, signal processing and antennas. This chapter builds upon that theory by describing how a radar antenna can be used as an imaging system. Having laid the foundation for understanding radar systems in general, this chapter introduces the synthetic aperture radar, which is the instrument of interest for this study. Of particular interest are the impulse response and resolution properties of such systems. The 2D impulse response shall be decoupled into the range and azimuth components, and the latter, on which the formalism of Raney is based, will be used in the following chapters for evaluating the theory and modelling a simple SAR system.

5.1 Basic principles

Consider a radar system mounted on a platform moving parallel to the ground. Such imaging systems are usually side-looking, i.e. it illuminates an area to one side of the nadir track, which is the system path projected onto the ground. A pulse is transmitted with a given frequency, and due to the side-looking configuration each pulse sweeps across the ground at the speed of light. Targets in the range direction are then discriminated by the time between the return pulses from the targets (Elachi & van Zyl, 2006, p. 239-255).

The ranging is done along the antenna boresight, i.e. the axis along which the antenna gain attains its maximum. This is referred to as the slant range. In order to measure distance along the ground the slant range has to be converted into ground range.

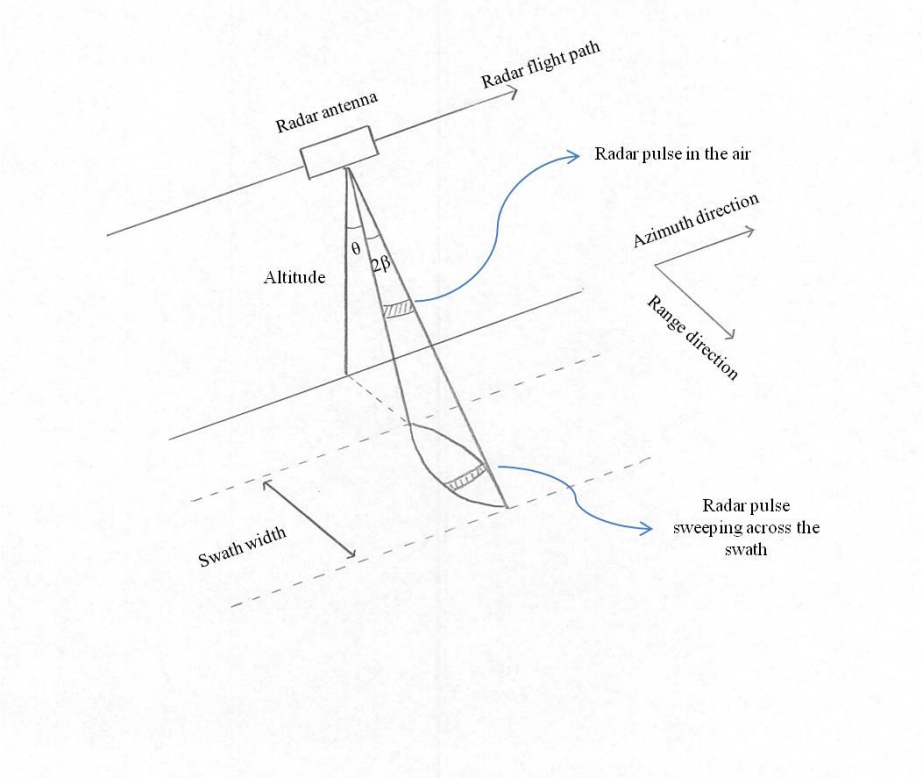

Figure 5.1: Geometry of a side-looking imaging radar, based on figure 6-15 and figure 6-25 in Elachi and van Zyl (2006). The radar antenna transmits pulses which sweep across the ground. Between pulses any echoes from illuminated targets are recorded.

Figure 5.1 shows the SAR geometry for a system with zero squint angle. The squint angle is defined as the angle between the slant range vector and the zero-Doppler plane. The zero-Doppler plane is in turn defined as the plane which extends from the antenna and has a normal vector equal to the platform velocity (Cumming & Wong, 2005, p. 117-120). The projection of the squint angle onto the ground corresponds to the beam yaw angle, which is constant, while the squint angle depends on the target range. For simplicity a zero squint angle shall be assumed henceforth.

The azimuth resolution of real aperture radar (RAR), i.e. the smallest distance between two separable objects, is equal to the width of the antenna footprint. This is in turn proportional to the radar wavelength and target range, and inversely proportional to the antenna length in the azimuth direction. Hence for a platform moving at an altitude R_0 with an azimuth antenna length L_a, look angle θ and radar wavelength λ, the corresponding azimuth resolution δ_a is given by:

$$\delta_a = \frac{R_0 \lambda}{L_a \cos\theta} \tag{5.1}$$

where $\frac{\lambda}{L}$ is the approximate antenna beam width in the azimuth direction.

For spaceborne radar with an altitude of around 800 km, this means that δ_a is typically hundred of meters or several kilometres. This type of system is therefore unsuitable for imaging from space.

A synthetic aperture radar solves this problem by using the Doppler history to synthesize a large aperture (Cumming & Wong, 2005, ch. 4). While a target stays in the radar beam it is illuminated by many pulses. As the satellite approaches the target, the radar signal is frequency modulated due to the relative motion between antenna and target, which results in a positive shift in frequency. When the radar passes directly above the target the frequency shift turns from positive to negative.

The increase in resolution is obtained by using the Doppler history of the target. Specifically, the return pulses recorded by the radar can be considered as a sampling of a continuous waveform which represents the Doppler-shifted return signal in the time domain. The frequency modulation introduces a phase shift:

$$\psi(\eta) = -\pi \frac{B_D}{T_a} \eta^2 \tag{5.2}$$

(Vachon, 1983, p. 6) where B_D is the Doppler bandwidth, T_a is the integration time, and η is the azimuth time referenced to the zero Doppler time.

This signal can be reconstructed if the pulse repetition frequency (PRF) ensures that the sampling rate is sufficiently high to avoid aliasing[1]. The radar signal can then be focused in the azimuth direction by matched filtering.

5.2 Data arrangement and processing

The echo of each pulse is recorded in between pulse transmission. This takes the form of a voltage at the antenna as a function of time, yielding a curve which represents the amplitude of the echo. One such curve is recorded for each pulse cycle. On a one-dimensional storage medium, the SAR data appears as a collection of voltage curves separated by gaps where the antenna is not recording. In a computer memory the voltage curves can instead be sampled and written as rows in a matrix. The first dimension of this matrix then corresponds to range time, while the second dimension corresponds to azimuth time. Rows and columns may be referred to as range lines and range gates respectively (Cumming & Wong, 2005, ch. 4.6.1).

The Doppler modulation described above, which is the key concept of a SAR system, encodes the signal from a target in a linear chirp along the azimuth direction. This is usually the case for the range direction as well due to the chosen structure of the transmitted pulse, as shall be further elaborated below. The job of a SAR processor is therefore to remove the chirp encoding in both range and azimuth in order to recover the signal from the target. Since the encoding can be expressed mathematically as two convolution along the two dimensions with the respective linear chirps, SAR processing is simply a demodulation process in two dimensions. However, it shall be shown that there is a dependency between azimuth time and range time which causes a significant complication.

This dependency shows up in the raw data in the form of range cell migration (RCM).

[1]The Shannon sampling theorem states that a continuous-time signal can be accurately reconstructed from a set of samples provided that the sampling rate is greater than the Nyquist rate, which is twice the maximum frequency of the sampled signal (McClellan et al., 2003, p. 77).

This effect is caused by the varying range to a target while it is observed in the radar beam. If the radar, travelling at a speed V, passes directly overhead of a target at a time $\eta = 0$, when the slant range distance is at a minimum R_0, then the slant range distance as a function of azimuth time is given by:

$$R(\eta) = R_0^2 + V^2\eta^2 \tag{5.3}$$

which, referring to figure 5.1, is obtained by the Pythagorean theorem. This in turn leads to a parabolic curving of the point target response, which has a convex shape towards the radar. The straightening of this parabola is referred to as range cell migration correction (RCMC). This is a challenging task, and therefore it is also a distinguishing feature of SAR processing algorithms (Cumming & Wong, 2005, p. 10).

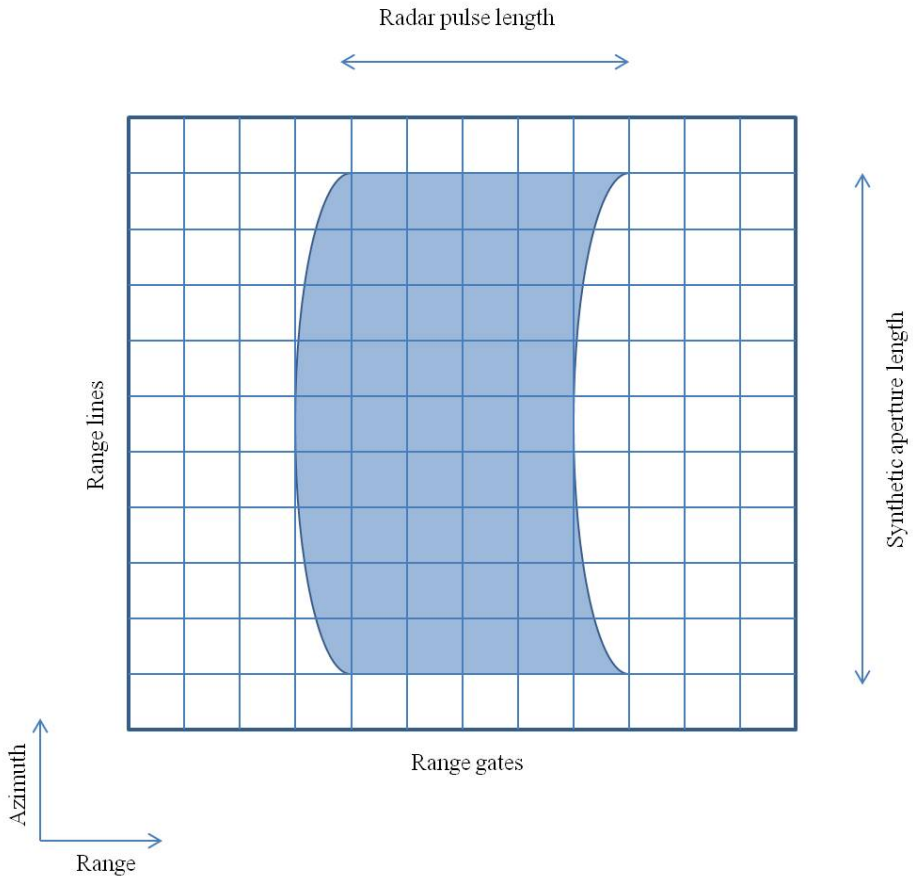

Figure 5.2: Locus of energy of the SAR point target response (not to scale). The shape may vary depending on the zero Doppler position. The grid represents range cells, i.e. sample points. Range cell migration can be considered significant if it occurs over at least one range cell. Based on figure 4.14 in Cumming and Wong (2005) and figure 6-41 in Elachi and van Zyl (2006).

While the modern literature on SAR processing techniques may give the impression that SAR systems require digital devices, this is not the case. A SAR image can also be focused by means of a series of lenses (Harger, 1970, ch. V). The first SAR images were formed with an optical correlator at the University of Michigan's Radar Laboratory in 1957, using coherent optics to compress chirped radar pulses (Galati, 2016; The Optical Society, 2005). The Seasat satellite, launched in 1978, carried a SAR instrument which transmitted data in real time to five ground stations in a 20

MHz analog data stream. The synthetic aperture, which was several kilometres long, was formed by means of an optical correlator, and the products were stored on 70 mm film. Approximately 10 percent of the roughly 42 hours[2] of SAR data which was collected by Seasat was digitally processed by NASA Jet Propulsion laboratory between 178 and 1982 (Alaska Satellite Facility, n.d.; Beal, Tilley, and Monaldo, 1983). Digital transmission of raw SAR data was first carried out on the Space Shuttle Columbia, which carried an imaging radar assembled from spare parts of the Seasat in the early eigthies (Jet Propulsion Laboratory, 2001).

5.3 Image fading

The amount of detail that can be recorded by an imaging system is limited by the resolution of the system. This limitation causes a phenomenon known as speckle in SAR images, which can be observed as a grainy noise pattern over an otherwise uniform surface. This phenomenon is caused by signal fading, which is the superposition of the returns from several scatterers which are simultaneously illuminated by the radar beam (Elachi & van Zyl, 2006, p. 242-248). The relative phase of the individual scatterers vary with viewing angle, which results in multiplicative noise in the radar image (Cumming & Wong, 2005, p. 265).

If each individual resolution cell in a scene is modelled as a discrete set of scatterers, the instantaneous voltage received at the radar sensor from one single cell can be expressed as:

[2]The Seasat mission ended 105 days after being launched due to a short circuit onboard the satellite. Interestingly, this event sparked rumours which claim that the failure was a deliberate action by the US military. Supposedly Seasat, being a civilian satellite, was too good at detecting submerged submarines, which in the context of the Cold War might cause embarrassment if such images were to be made public (Norris, 2008, p. 172).

$$V = V_e\, e^{i\varphi} = \sum_{n=1}^{N_s} V_n\, e^{i\varphi_n} \tag{5.4}$$

Suppose that $N_s \gg 1$ and that V_n and φ_n are independent random variables. If φ_n is uniformly distributed in the range $[-\pi, \pi]$, then the sum over the individual scatterers can be considered as a random walk in the complex plane due to the vectorial property of addition in $\mathbb{C}$.

Under these assumptions the observed amplitude V_e will have a Rayleigh distribution with some parameter s (which is dependent on the target, and therefore specific to each individual pixel) determined by the moments of the observed voltage, while the real and imaginary components of V will be independent identically distributed (iid) Gaussian random variables with zero mean and variance $\frac{s}{2}$. The observed phase φ will be uniformly distributed over $[-\pi, \pi]$ (Oliver & Quegan, 2004, p. 84-99).

The observed power is proportional to the square of the observed voltage, Making the change of variables $P = V^2$, the probability density function (pdf) of P is exponential with mean σ. Changing variables again to $P = s\,N$, the pdf of N is given by:

$$f_N(n) = e^{-n}, \quad n \geq 0 \tag{5.5}$$

This result explains the classification of speckle as multiplicative noise in that the observed power is expressed as a deterministic value s multiplied by an exponentially distributed random variable with mean 1. The parameter s is therefore proportional to the RCS of a point target introduced in equation 4.7 in section 4.2. In the case of a continuous extended target, suppose that the phase of the scattered signal is approximately constant over an area A. The quantity corresponding to the RCS for this extended target over the area A is then referred to as the differential backscattering coefficient, or normalized radar cross section (NRCS), denoted by σ^0 (Oliver & Quegan, 2004, p. 31), which is given by a slight modification to equation 4.7:

$$\texttt{Re-radiated power} = \frac{P_t G_t \sigma^0}{4\pi R^2} \tag{5.6}$$

Direct comparison of images from different SAR systems requires calibrating the images to σ^0, which is the physical quantity of interest.

5.4 Demodulation

The pulse transmitted by a SAR system is commonly a linear FM pulse, given by:

$$s_{pulse} = w_r(\tau) \cos\left(2\pi f_0 \tau + \pi K_r \tau^2\right) \tag{5.7}$$

where:

$$w_r(\tau) = \text{rect}\left(\frac{\tau}{T_r}\right) \tag{5.8}$$

is an approximation of the envelope of the pulse[3], K_r is the chirp FM rate, T_r is the pulse duration, and τ is the range time referenced to the centre of the pulse. The reflected energy $s_r(\tau)$ is a convolution of the ground reflectivity $g_r(\tau)$ with the pulse (Cumming & Wong, 2005, ch. 4.4).

For a point target at a distance R_a, $g_r(\tau) = A_0'\delta(\tau - \frac{2R_a}{c})$. Here A_0' models the backscatter coefficient and $\frac{2R_a}{c}$ is the delay time of the signal. Hence:

$$s_r(\tau) = A_0' w_r\left(\tau - \frac{2R_a}{c}\right) \cos\left(2\pi f_0\left(\tau - \frac{2R_a}{c}\right) + \pi K_r\left(\tau - \frac{2R_a}{c}\right)^2 + \psi\right) \tag{5.9}$$

where the variable ψ has been introduced to account for a possible phase change in the reflected signal due to scattering processes in the reflecting medium and the atmosphere[4].

To remove the carrier signal, the process of quadrature demodulation is applied (Cumming & Wong, 2005, ch. 4B.1).

[3]The function $rect(x)$ is by definition equal to 1 if $|x| \leq \frac{1}{2}$ and zero otherwise.

[4]Ignoring any associated reduction in signal strength.

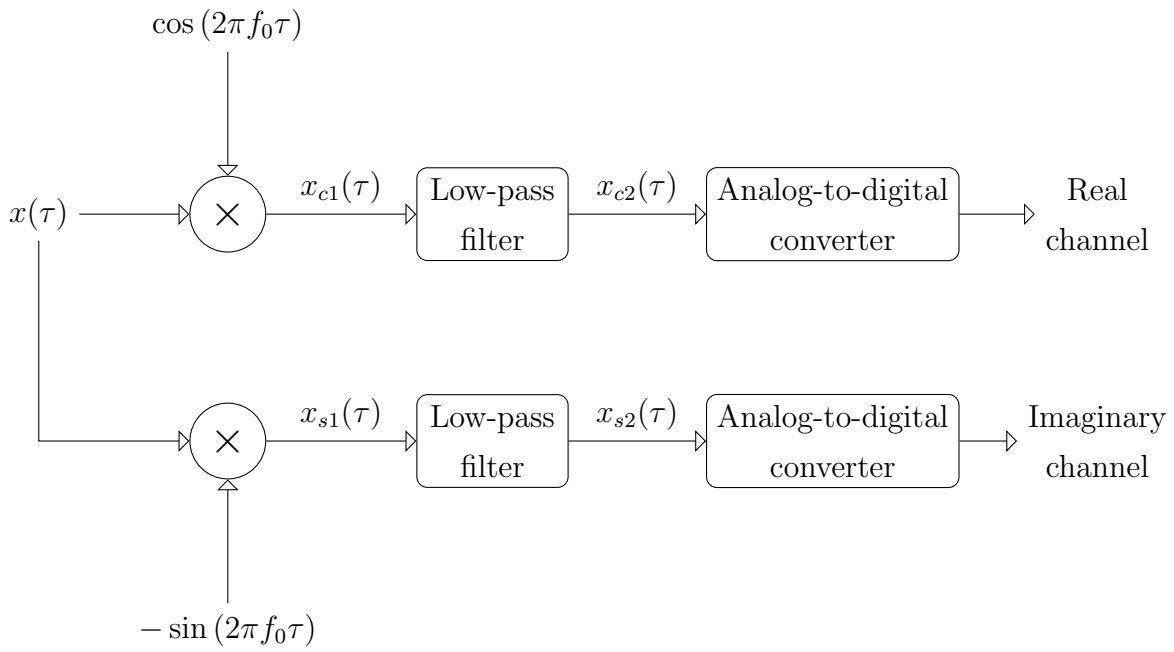

Figure 5.3: Diagram of quadrature demodulation to remove carrier signal. Based on figure 4B.1 in Cumming & Wong (2005).

This process is based on the trigonometric identities:

$$\cos\theta\cos\varphi = \frac{1}{2}\left(\cos\left(\theta-\varphi\right)+\cos\left(\theta+\varphi\right)\right) \tag{5.10}$$

$$\sin\theta\cos\varphi = \frac{1}{2}\left(\sin\left(\theta-\varphi\right)+\sin\left(\theta+\varphi\right)\right) \tag{5.11}$$

The output of the two multipliers in figure 5.3 is therefore:

$$x_{c1}(\tau) = \frac{1}{2}\cos\varphi(\tau) + \frac{1}{2}\cos 4\pi f_0\tau + \varphi(\tau) \tag{5.12}$$

$$x_{s1}(\tau) = \frac{1}{2}\sin\varphi(\tau) + \frac{1}{2}\sin 4\pi f_0\tau + \varphi(\tau) \tag{5.13}$$

$$\tag{5.14}$$

where $\varphi(\tau)$ is the frequency modulation. Since f_0 is much higher than $\varphi(\tau)$, the second term in $x_{c1}(\tau)$ and $x_{c2}(\tau)$ are filtered out by the low-pass filter, and the resulting complex signal is:

$$x_{out}(\tau) = x_{c2}(\tau) + ix_{s2}(\tau) = \frac{1}{2}e^{i\varphi(\tau)} \tag{5.15}$$

By inspection of equation 5.9, $\varphi(\tau)$ for a point target is:

$$\varphi(\tau) = -\frac{4\pi f_0 R(\eta)}{c} + \pi K_r \left(\tau - \frac{2R(\eta)}{c}\right)^2 + \psi \tag{5.16}$$

where R is now a function of azimuth time η. Finally, the demodulated baseband signal is then:

$$s(\tau, \eta) = A_0' e^{i\psi} w_r \left(\tau - \frac{2R(\eta)}{c}\right) w_a(\eta - \eta_c) e^{-i4\pi f_0 \frac{R(\eta}{c} + i\pi K_r \left(\tau - \frac{2R(\eta)}{c}\right)^2} \tag{5.17}$$

where:

$$w_a(\eta) = \text{sinc}^2\left(\frac{0.886\theta(\eta)}{\beta}\right) \tag{5.18}$$

is the azimuth antenna pattern which relates the received signal strength to the angle θ from the boresight and the antenna azimuth beamwidth β (Cumming & Wong, 2005, p. 138 and p. 144).

5.5 SAR impulse response

If the factor $A_0' e^{i\psi}$ in equation 5.17 is ignored, then what is left is the impulse response $h(\tau, \eta)$ of the SAR system since this expression is the baseband signal received from a point target. Hence:

$$h(\tau, \eta) = w_r \left(\tau - \frac{2R(\eta)}{c}\right) w_a(\eta - \eta_c) e^{-i4\pi f_0 \frac{R(\eta)}{c} + i\pi K_r \left(\tau - \frac{2R(\eta)}{c}\right)^2} \tag{5.19}$$

Knowing the impulse response, the baseband return signal from any ground surface with known reflectivity $g(\tau, \eta)$ can be worked out by a simple convolution:

$$s_{bb}(\tau, \eta) = g(\tau, \eta) * h(\tau, \eta) + n(\tau, \eta) \tag{5.20}$$

where $n(\tau, \eta)$ accounts for the additive noise of the system, e.g. thermal noise, which can be modelled (Cumming & Wong, 2005, ch. 4.6.3). A diagram representing the SAR system model found in equation 5.20 is shown in figure 5.4.

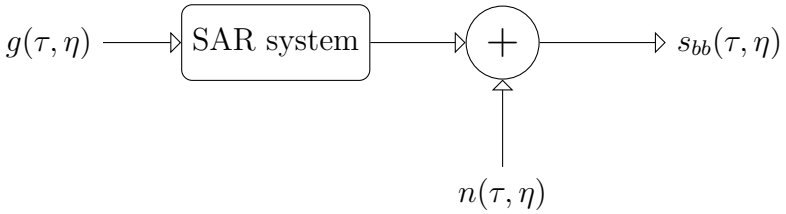

Figure 5.4: Model of a SAR system with additive noise. Based on figure 4.15 in Cumming & Wong (2005).

The aim of SAR processing is to recover $g(\tau, \eta)$, which in this system model is a deconvolution process.

5.6 Range resolution

If the signal:

$$x(t) = \text{rect}\left(\frac{t}{T}\right) e^{i\pi K t^2} \tag{5.21}$$

is transmitted and its echo received at a time t_0 later, then the echo is given by:

$$x_r(t) = \text{rect}\left(\frac{t - t_0}{T}\right) e^{i\pi K (t - t_0)^2} \tag{5.22}$$

The matched filter[5] $h(t)$ to $x(t)$ is obtained by time-reversal and complex conjugation:

$$h(t) = \text{rect}\left(\frac{t}{T}\right) e^{-i\pi K t^2} \tag{5.23}$$

[5]In section 3.2 the letter h was used to denote the impulse response of an LTI system. Since a matched filter is an LTI system, it shall throughout this thesis be denoted by the same letter, following the notation of McClellan et al. (2003). The system characterized by the function h will be made clear from context.

The pulse compression consists of calculating the convolution between $x_r(t)$ and $h(t)$. This convolution is referred to as the correlation function between the two signals, which is approximated by:

$$x(t) * h(t) \approx T \operatorname{sinc}\left(KT(t - t_0)\right) \tag{5.24}$$

The peak of this sinc function marks the location of the original signal in the echo (Cumming & Wong, 2005, ch. 3.3). The condition for 5.24 to be valid is that the time bandwidth product (TBP)[6] is larger than 100 (Cumming & Wong, 2005, p. 108-110). This can be understood by noting that:

$$x(t) * h(t) = (T - |t|) \operatorname{rect}\left(\frac{t}{2T}\right) \operatorname{sinc}(Kt(T - |t|)) \tag{5.25}$$

where $(T - |t|) \operatorname{rect}\left(\frac{t}{2T}\right)$ represents a triangular envelope while $\operatorname{sinc}(Kt(T - |t|))$ resembles the sum of three sinc functions separated by an interval T. This is illustrated in figure 5.5. The condition that TBP ≥ 100 ensures that the two outer sinc functions are sufficiently narrow not to interfere with the one centred at $t = 0$.

[6]The TBP is defined as *"the product of the 3-dB width in time and the 3-dB bandwidth of the signal"* (Cumming & Wong, 2005, p. 35).

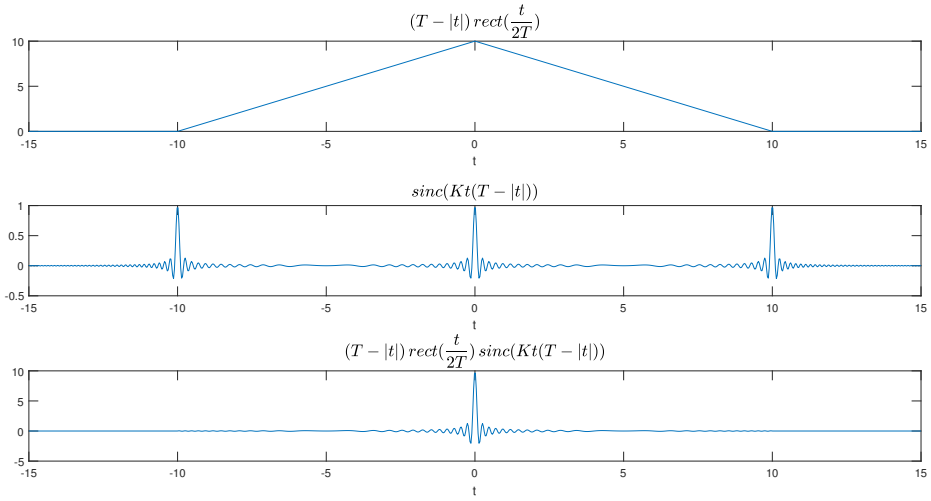

Figure 5.5: Reproduction of figure 3A.1 in (Cumming & Wong, 2005), which shows the separate factors in a matched filter output. Here $K = 1$ and $T = 10$. The TBP is equal to $|K|T^2$ (Cumming & Wong, 2005, p. 71), which in this case is 100.

The pulse resolution is defined as *"the spread between the two -3-dB points of the compressed signal"* (Cumming & Wong, 2005, p. 83), and is given by:

$$\delta_t = \frac{0.886}{|K|T} \tag{5.26}$$

where the constant 0.886 appear for the same reason as in appendix A. In order to convert this to resolution in the slant range, δ_t is multiplied by the speed of propagation (in this case the speed of light c) and divided by 2 to account for the two-way travel distance:

$$\delta_r = \frac{0.886c}{2|K_r|T_r} \tag{5.27}$$

Cumming and Wong (2005, p. 83 ad 131) note that the constant 0.886 can be ignored if a window is applied to the signal. In this case there will be an additional factor $\gamma_{w,r}$, which Cumming and Wong (2005, p. 92) refer to as a impulse response width (IRW) broadening factor.

5.7 Azimuth resolution

Cumming and Wong (2005, p. 140-149) gives the obtainable azimuth resolution as:

$$\delta_a = \frac{0.886 V_g \cos\theta_{r,c}}{\Delta f_d}\gamma_{w,a} = \frac{L}{2}\frac{V_g}{V_s}\gamma_{w,a} \tag{5.28}$$

where V_g is the speed of the antenna footprint along the ground, V_s is the satellite speed, L is the antenna length, and $\gamma_{w,a}$ is the azimuth IRW broadening factor. The angle $\theta_{r,c}$ is an approximation to the squint angle at the zero Doppler time c, and the doppler bandwidth Δf_d is given by:

$$\Delta f_D = \frac{2V_s \cos\theta_{r,c}}{\lambda}\beta_a = 0.886\frac{2V_s \cos\theta_{r,c}}{L} \tag{5.29}$$

with the azimuth FM rate of change K_a being:

$$K_a = \frac{2V_r^2 \cos^2\theta_{r,c}}{\lambda R_0} \tag{5.30}$$

Here V_r is the speed obtained by a rectilinear approximation to the curved Earth geometry (Cumming & Wong, 2005, figure 4.6), which shall prove useful in later chapters.

They also note that the achievable azimuth resolution is normally given as half the antenna length since:

$$\gamma_{w,a}\frac{V_g}{V_s} \approx 1 \tag{5.31}$$

for small squint angles.

(Elachi & van Zyl, 2006, p. 249-255) ignores the squint angle altogether and derives the azimuth resolution by two different approaches.

The synthetic array approach exploits the equivalence between a moving antenna and an antenna array, provided that the received signals are recorded coherently and that the target is static while seen by the antenna. The maximum width of the antenna

footprint created by the synthesized array is equal to twice the width of the real footprint since the target must stay within the beam during the synthesis. Recalling equation 5.1, the synthetic footprint then has a maximum width $\mathcal{L}$ of:

$$\mathcal{L} = \frac{2\lambda R_0}{L_a} \tag{5.32}$$

Taking the beamwidth to be:

$$\beta_s = \frac{\lambda}{\mathcal{L}} = \frac{L_a}{2R_0} \tag{5.33}$$

the resulting array footprint is:

$$\delta_a = R_0\beta_a = \frac{L_a}{2} \tag{5.34}$$

which is in agreement with the result obtained by Cumming and Wong (2005). It should be noted that Elachi and van Zyl (2006, p. 251) states equality in equation 5.34. However, the expression $h\beta_s$ is, by the definition of the radian, the arclength of a segment of a circle with radius h, spanned over an angle β_s. Hence this result should be taken as an approximation as well.

Alternatively, the doppler synthesis approach uses the Doppler bandwidth to derive the same expression. The echo from a target has a spectrum which spans the interval $f_0 \pm f_D$. As the radar approaches a target, the radial speed of the satellite towards the target causes a phase shift. Every shift of $\frac{\lambda}{2}$ each way leads to a total displacement of one wavelength, which corresponds to 2π radians or one complete cycle (Kingsley & Quegan, 1992, p. 19-20). Hence the phase shift is the radial speed V_{rad} divided by $\frac{\lambda}{2}$:

$$f_D = \frac{2V_{rad}}{\lambda} \tag{5.35}$$

The radial speed between the satellite and a target just entering the beam is the projection $V_s \sin\frac{\beta_a}{2}$, and f_D is therefore given by:

$$f_D = \frac{2V_s}{\lambda}\sin\frac{\beta_a}{2} \tag{5.36}$$

and using the small angle approximation and the approximate beamwidth in equation 4.20:

$$f_D \approx \frac{V_s \beta_a}{\lambda} = \frac{V_s}{L_a} \tag{5.37}$$

and the Doppler bandwidth is $2f_D$. Two targets displaced by a distance δ_a in the azimuth direction will have a time displacement:

$$\Delta\eta = \frac{\delta_a}{V_s} \tag{5.38}$$

The shortest observable time displacement by the SAR system is the inverse of the Doppler bandwidth:

$$\Delta\eta_{min} = \frac{1}{2f_D} = \frac{L_a}{2V_s} \tag{5.39}$$

and by plugging this into equation 5.38 the finest obtainable resolution is obtained:

$$\delta_a = V_s \Delta\eta_{min} = \frac{L_a}{2} \tag{5.40}$$

5.8 Azimuth phase shifting

Since the distance between satellite and target varies while the target is within the radar beam, there will be a phase difference between two return signals in the same manner as for the two point radiators in section 4.3. i.e. the radar wave number times the path difference, and in this case multiplied by two due to the two-way travel. Hence, when the radar is at position x_i along the flight path while observing a target at a radial distance r_i:

$$\varphi_i = 2k\left(r_i - R_0\right) = \frac{4\pi\left(r_i - R_0\right)}{\lambda} \tag{5.41}$$

This phase should therefore be subtracted from each echo in order to achieve the highest possible resolution, the process of which is referred to as focusing (Elachi &

van Zyl, 2006, p. 251-253).

An unfocused SAR can simplify the processing. Assuming that phase shifts of less than $\frac{\lambda}{4}$ can be neglected, the corresponding synthetic array length can be solved by combining equation 5.41 with the pythagorean theorem to obtain:

$$2k\left(\sqrt{R_0^2+\left(\frac{L_a}{2}\right)^2}-R_0\right)=\frac{\pi}{4} \tag{5.42}$$

By noting that the first order Taylor expansion of $\sqrt{1-x}$ is $1-\frac{x}{2}$ and assuming $R_0 \gg 1$, this can be solved approximately:

$$\begin{aligned} 2k\left(\sqrt{R_0^2+\left(\frac{L_a}{2}\right)^2}-R_0\right) &= 2k\left(R_0\left(\sqrt{1-\frac{L_a^2}{4R_0^2}}-1\right)\right) \\ &\approx 2kR_0\left(1-\frac{1}{2}\frac{L_a^2}{4R_0^2}-1\right) \\ &= \frac{\pi L_a^2}{\lambda R_0} \end{aligned} \tag{5.43}$$

Therefore:

$$\frac{\pi L_a^2}{\lambda R_0}=\frac{\pi}{4} \implies L_a=\sqrt{\frac{\lambda R_0}{2}} \tag{5.44}$$

and the resulting resolution is:

$$\delta_a=\frac{\lambda R_0}{L}=\sqrt{2\lambda R_0} \tag{5.45}$$

5.9 Azimuth processing model

The pulse scanning along the range direction travels at the speed of light, while the the scanning in the azimuthal direction proceeds at the speed of the SAR carrier. These two speed are vastly different in magnitude, with the range scanning being

virtually instantaneous in comparison with the azimuth scanning speed.

Cumming and Wong (2005) stress that the SAR impulse response depends on both range and azimuth time, which complicates the deconvolution. On the other hand, Massonet and Souyris (2008, ch. 3.12) treat the impulse responses in the azimuth and range directions separately.

The impulse response in the range direction is simply taken to be the time-shifted chirp pulse:

$$h_r(\tau) = \text{rect}\left(\frac{\tau - \tau_0}{T_r}\right) e^{i\pi K(\tau-\tau_0)^2} \tag{5.46}$$

where T_r is the pulse length, which corresponds to equation 3.31 in (Cumming & Wong, 2005, p. 86) with zero time offset. Similarly, the azimuth impulse response is taken to be the chirp generated by the Doppler effect:

$$h_a(\eta) = \text{rect}\left(\frac{\eta}{T_a}\right) w_a(\eta) e^{-\frac{i\pi B_D \eta^2}{T_a}} \tag{5.47}$$

where B_D is the Doppler bandwidth and $\eta = 0$ at the point of closest approach to the target. Although not stated, a zero squint angle and zero Doppler centroid frequency must be assumed. This approach ignores range migration, but results in a decoupling of the impulse response so that the range and azimuth channels can be processed

separately[7]

A moving target does not complicate range processing due to the difference in magnitude between pulse propagation speed and target motion, while the azimuth scanning speed is on the same scale. This channel is therefore severely affected by target motion (Vachon, 1983, ch. 2.1).

Figure 5.6 describes the model for the azimuth channel used by Vachon (1983). Here f represents the input to the radar antenna as a function of azimuth time η. This signal is modified by convolution with a prefilter w, which accounts for the antenna azimuth pattern and Doppler modulation. Receiver noise n is added before the signal goes through the processor h. The image g is then obtained by a squaring the magnitude of the processor output.

[7]It appears that different authors use different signs in the exponent in equation 5.47. Recalling equation 5.2, the rate of change is negative, which agrees with Vachon (1983) and Kingsley and Quegan (1992), while Massonet and Souyris (2008) and Cumming and Wong (2005) use a positive rate and Raney (1980b) uses both. This is dependent upon the local coordinate system and should not make any difference for modelling purposes since the sign merely determines the direction of rotation of the phasor in the complex plane, and as long as the matched filter is correctly constructed the final output should be unaffected. However, from a physical point of view it can be argued that the rate should be negative if η is taken to be negative during the radar's approach to the target and positive as the target recedes. The derivative of equation 5.2 then changes sign from positive to negative at $\eta = 0$. This is consistent with the frequency shift observed for a sound source moving at an angle relative to the observer.

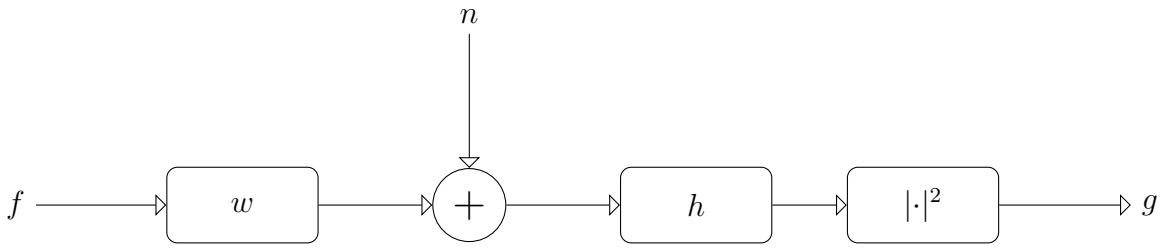

Figure 5.6: Block diagram describing a model of the SAR azimuth channel. Based on figure 1 in Vachon (1983).

The output image g of a single range gate can therefore be expressed as:

$$g(\eta) = |f(\eta) * w(\eta) * h(\eta) + n(\eta) * h(\eta)|^2 \tag{5.48}$$

Recalling the expression for the Doppler modulation (equation 5.2), the prefilter w is given by:

$$w(\eta) = w_a(\eta) \cdot e^{-i\pi \frac{B_D}{T_a} \eta^2} \tag{5.49}$$

where $w_a(\eta)$ is the azimuthal antenna pattern. The processor is typically a matched filter $h(\eta) = w^*(-\eta)$, which is the optimum SR processor for a point target assuming additive Gaussian noise (Raney, 1980b, p. 777).

This processing model is consistent with the azimuth compression step in the basic range Doppler algorithm (RDA). In this algorithm the raw SAR data is first compressed in the range direction by means of a filter matched to the range chirp (equation 5.46), either directly by a convolution or in the frequency domain after a range FFT. In the latter case the inverse FFT is applied after filtering. In the next step the azimuth FFT is applied, which transforms the data into the range Doppler domain where range cell migration correction is performed. Assuming the correction is perfect, the trajectory of each target will run parallel to the azimuth frequency axis, such that azimuth compression can be done by a filter matched to the azimuth chirp (equation 5.47), either in the frequency domain prior to the inverse FFT or by

a convolution afterwards (Cumming & Wong, 2005, p. 225-228).

The rest of this thesis will focus on the azimuth compression step, and it shall therefore be assumed that the range compression and RCMC have already been performed.

Chapter 6

Quadratic filter theory

The following chapter refers to Raney (1969a), who proposes a method for linearizing quadratic functionals. In this formalism an N-dimensional non-linear problem is exchanged for a $2N$-dimensional linear one, where N is the number of temporal dimensions. This procedure allows the properties of LTI-systems, which were covered in chapter 3, to be exploited. This shall be done in subsequent chapters by introducing an additional azimuth time dimension during processing in order to take advantage of the scene coherence time.

The aim of this chapter is to offer a complete proof for the formalism. Some of the derivations are not to be found in Raney's articles, and one contribution of this study is to supply these in order to provide a unified presentation of the formalism. It is hoped that this may prove useful for other purposes that are beyond the scope of this study as well.

6.1 Motivation

In figure 5.6 the final image is the squared norm of the processor output. Suppose that the PRF is sufficiently high such that the Doppler spectrum can be perfectly reconstructed from the sampling process. Then the sampling process can be disregarded altogether and the azimuth time can be treated as a continuous variable.

Raney (1980b, p. 777) refers to this as the continuous-wave model, where the scene reflects a continuous signal which in this case is presented to the azimuth processing channel. Therefore equation 5.48 can be evaluated be means of convolution integrals. The impulse response is then[1]:

$$\begin{aligned} g(\eta) &= |w(\eta) * h(\eta)|^2 \\ &= \left| \int w(x)\, h(\eta - x)\, dx \right|^2 \\ &= \int w(x)\, h(\eta - x)\, dx \left(\int w(y)\, h(\eta - y)\, dy \right)^* \\ &= \int w(x)\, h(\eta - x)\, dx \int w^*(y)\, h^*(\eta - y)\, dy \\ &= \iint h(\eta - x)\, h^*(\eta - y)\, w(x) w^*(y)\, dx\, dy \\ &\equiv \iint Q(\eta - x, \eta - y)\, w(x) w^*(y)\, dx\, dy \end{aligned} \tag{6.1}$$

where $Q(\eta - x, \eta - y) \equiv h(\eta - x)\, h(\eta - y)$. The properties of the last integral is the subject of quadratic filter theory.

6.2 Definition

A quadratic filter Q is here defined by the relation:

$$g(u) = \iint_T Q(u - x, u - y) f(x) f^*(y)\, dx\, dy \tag{6.2}$$

which relates an input f to the output g of a non-linear time-invariant system characterized by the impulse response Q.

It is required that Q be a correlation function. This requirement puts a number of constraints on Q, first among which is:

$$Q(x, y) = Q^*(y, x) \tag{6.3}$$

[1]The limits of integrals will be omitted in the cases where the domain of integration is $\mathbb{R}$.

which Raney refers to as *"complex (Hermitian) symmetric"*, but which more correctly describes Q as a Hermitian form (Barile, n.d.). Furthermore, Q should be square integrable:

$$\iint_T |Q(x,y)|^2 \, dx \, dy < \infty \tag{6.4}$$

and also positive definite, such that:

$$\iint_T Q(x,y)s(x)s^*(y) \, dx \, dy \geq 0 \tag{6.5}$$

for any square integrable function s. Finally, it is required that:

$$\int Q(x,x) < \infty \tag{6.6}$$

6.3 Frequency domain representation

The representation of equation 6.2 in the frequency domain is obtained by means of the Fourier transform. Consider the change of variables:

$$\begin{aligned} s &= u - x \\ t &= u - y \end{aligned} \tag{6.7}$$

Then equation 6.2 takes the form:

$$g(u) = \iint_{T'} Q(s,t)f(u-s)f^*(u-t) \, ds \, dt \tag{6.8}$$

Let $\tilde{g}(\omega) = \mathcal{F}[g(u)]$. Then:

$$\tilde{g}(\omega) = \int g(u)e^{-i\omega u} \, du = \frac{1}{2\pi} \int \tilde{Q}(\lambda, \omega - \lambda)\tilde{f}(\lambda)\tilde{f}^*(\lambda - \omega) \, d\lambda \tag{6.9}$$

Proof.

$$\begin{aligned}\tilde{g}(\omega) &= \mathcal{F}\left[\iint_{T'} Q(s,t) f(u-s) f^*(u-t)\, ds\, dt\right] \\ &= \iint_{T'} Q(s,t) \mathcal{F}\left[f(u-s) f^*(u-t)\right]\, ds\, dt\end{aligned} \tag{6.10}$$

The Fourier transform of a product is a convolution, scaled by 2π, and therefore:

$$\mathcal{F}\left[f(u-s) f^*(u-t)\right] = \frac{1}{2\pi} \mathcal{F}[f(u-s)] * \mathcal{F}[f^*(u-t)] \tag{6.11}$$

Furthermore, a time delay of t_d gives rise to an exponential $e^{-i\omega t_d}$ in the Fourier transform, and $f^*(t) \leftrightarrow \tilde{f}^*(-\omega)$, such that:

$$\begin{aligned}\mathcal{F}[f(u-s)] * \mathcal{F}[f^*(u-t)] &= \left(e^{-i\omega s} \tilde{f}(\omega)\right) * \left(e^{-i\omega t} \tilde{f}^*(-\omega)\right) \\ &= \int e^{-i\lambda s} \tilde{f}(\lambda)\, e^{-i(\omega-\lambda)t} \tilde{f}^*\left(-(\omega-\lambda)\right)\, d\lambda \\ &= \int e^{-i\lambda s} e^{-i(\omega-\lambda)t} \tilde{f}(\lambda)\, \tilde{f}^*(\lambda-\omega)\, d\lambda\end{aligned} \tag{6.12}$$

Plugging this back into equation 6.10, exchanging the order of integration and letting $T' = \mathbb{R}^2$:

$$\begin{aligned}\tilde{g}(\omega) &= \frac{1}{2\pi} \iint_{T'} Q(s,t) \left(\int e^{-i\lambda s} e^{-i(\omega-\lambda)t} \tilde{f}(\lambda)\, \tilde{f}^*(\lambda-\omega)\, d\lambda\right) ds\, dt \\ &= \frac{1}{2\pi} \int \left(\iint_{T'} Q(s,t) e^{-i\lambda s} e^{-i(\omega-\lambda)t}\, ds\, dt\right) \tilde{f}(\lambda)\, \tilde{f}^*(\lambda-\omega)\, d\lambda \\ &= \frac{1}{2\pi} \int \tilde{Q}(\lambda, \omega-\lambda) \tilde{f}(\lambda)\, \tilde{f}^*(\lambda-\omega)\, d\lambda\end{aligned} \tag{6.13}$$

■

6.4 Augmentation of variables

The motivation of Raney (1969a) is to express this relation in a form which corresponds to the transfer function for a linear filter. This is done by augmenting variables, resulting in what Raney refers to as a dilinear extension of g. This is represented by:

$$g(u) \to G(u, v) \tag{6.14}$$

where $G(u, v)$ is defined as:

$$G(u, v) = \iint_{T'} Q(x, y) f(u - x) f^*(v - y)\, dx\, dy \tag{6.15}$$

which can be recognized as a two-dimensional convolution. Hence Q is now the impulse response of an LTI system. Taking the Fourier transform and letting $T' = \mathbb{R}^2$:

$$\tilde{G}(\omega, \lambda) = \tilde{Q}(\omega, \lambda) \tilde{f}(\omega) \tilde{f}^*(-\lambda) \tag{6.16}$$

Proof.

$$\begin{aligned}
\tilde{G}(\omega, \lambda) &= \iint \left(\iint_{T'} Q(x, y) f(u - x) f^*(v - y)\, dx\, dy \right) e^{-i\omega u} e^{-i\lambda v}\, du\, dv \\
&= \iint_{T'} Q(x, y) \left(\int f(u - x) e^{-i\omega u}\, du \int f(u - x) e^{-i\lambda v}\, dv \right) dx\, dy \\
&= \tilde{f}(\omega) \tilde{f}^*(-\lambda) \iint_{T'} Q(x, y) e^{-i\omega x} e^{-i\lambda y}\, dx\, dy \\
&= \tilde{Q}(\omega, \lambda) \tilde{f}(\omega) \tilde{f}^*(-\lambda)
\end{aligned} \tag{6.17}$$

■

Hence this extension allows the quadratic filter to be described in the frequency domain by a linear two-dimensional transfer function.

In order for this to be useful, it is required that the observable output $g(u)$ can be recovered from $\tilde{G}(\omega, \lambda)$. (Raney, 1969a) does not provide a complete proof of this assertion, but rather refers to an operation called association of variables, here defined as:

$$\tilde{q}(\omega) = \frac{1}{2\pi} \int Q(\omega - \lambda, \lambda)\, d\lambda = \frac{1}{2\pi} \int \tilde{Q}(\eta, \omega - \eta)\, d\eta \qquad (?) \tag{6.18}$$

where $q(x) = Q(x, x)$. This, Raney informs, can be derived from the definition of the inverse Fourier transform of $\tilde{Q}(\omega, \lambda)$ by a change of variables. The second equality is

rather puzzling since the two integrals are related by a linear change of variables, yet involve the Fourier transform pair Q and $\tilde{Q}$, such that ω appears in the spatial domain.

The answer can be found in the appendix of Raney (1981a), where the same relation is given as:

$$\tilde{q}(\omega) = \frac{1}{2\pi} \int \tilde{Q}(\omega - \lambda, \lambda)\, d\lambda = \frac{1}{2\pi} \int \tilde{Q}(\eta, \omega - \eta)\, d\eta \tag{6.19}$$

which is formally correct and confirms that there is indeed an error in equation 16 in Raney (1969a).

Proof.

$$\begin{aligned}
\tilde{q}(\omega) &= \int q(x) e^{-i\omega x}\, dx \\
&= \int Q(x, x) e^{-i\omega x}\, dx \\
&= \int \mathcal{F}^{-1}\left[\tilde{Q}(\eta, \lambda)\right] e^{-i\omega x}\, dx \\
&= \int \left(\iint \frac{1}{4\pi^2} \tilde{Q}(\eta, \lambda) e^{i\eta x} e^{i\lambda y}\, d\eta\, d\lambda \right) e^{-i\omega x}\, dx \\
&= \frac{1}{4\pi^2} \iint \tilde{Q}(\eta, \lambda) \left(\int e^{i(\eta + \lambda - \omega)x}\, dx \right) d\eta\, d\lambda
\end{aligned} \tag{6.20}$$

The integral over x is the inverse Fourier transform of 1 if x is taken to be the frequency. Using the transform pair $1 \leftrightarrow 2\pi\delta(\omega)$ (McClellan et al., 2003, table 11-2):

$$\tilde{q}(\omega) = \frac{1}{4\pi^2} \iint \tilde{Q}(\eta, \lambda) \cdot 2\pi\delta(\eta + \lambda - \omega)\, d\eta\, d\lambda \tag{6.21}$$

Due to the sampling property of the Dirac delta, the only contribution to the integral over λ comes from the point where $\lambda = \omega - \eta$:

$$\tilde{q}(\omega) = \frac{1}{2\pi} \int \tilde{Q}(\eta, \omega - \eta)\, d\eta \tag{6.22}$$

Finally, the change of variables $\eta = \omega - \lambda$ yields the second equality in equation 6.19. ■

Having established association of variables as a valid operation, Raney (1981a) completes the concept by showing that $g(u)$ can be recovered from $\tilde{g}(\omega)$. Applying association of variables to $\tilde{g}(\omega)$ and using equation 6.16:

$$\begin{aligned} \tilde{g}(\omega) &= \frac{1}{2\pi} \int \tilde{G}(\eta, \omega - \eta)\, d\eta \\ &= \frac{1}{2\pi} \int \tilde{Q}(\eta, \omega - \eta) \tilde{f}(\eta) \tilde{f}^*(\eta - \omega)\, d\eta \end{aligned} \tag{6.23}$$

Comparing this with equation 6.9, it can be verified that this result is identical to the one obtained by taking the Fourier transform of $g(u)$ directly.

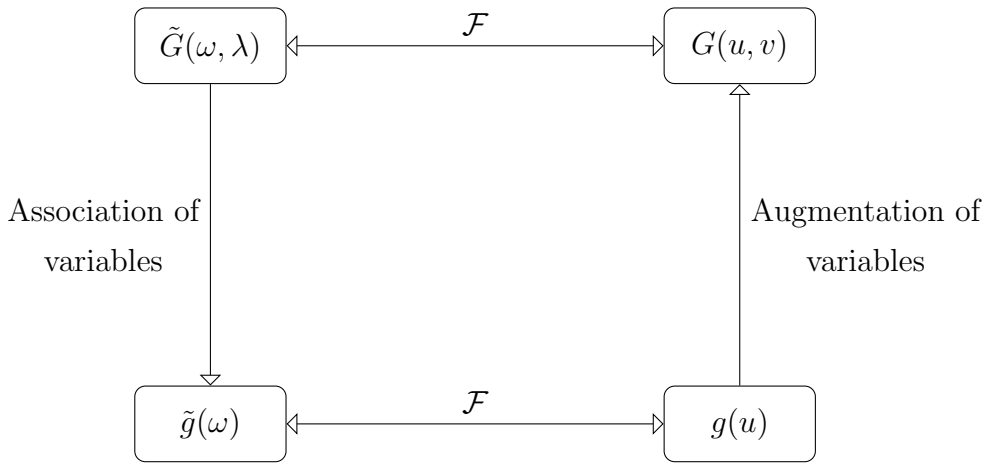

Figure 6.1: Flowchart describing the mapping of the output $g(u)$ of a quadratic filter to a two-dimensional domain. Based on Raney (1981a).

Chapter 7

Partially coherent targets

This chapter commences by providing a thorough discussion of the concept of coherence, which originates in classical optics. This shall therefore be the starting point, and the connection to partially coherent SAR systems shall be made. A system model for such systems shall then be presented, and the theory of quadratic filters from the previous chapter will be applied following Raney(1980a, 1980b, 1981a). Finally the validity of this approach shall be discussed, which forms part of the contribution of this study to the topic.

7.1 Coherence

The concept of coherence is central to this study and must be carefully defined in order to proceed. A natural starting point for this is the field of optics.

In Young's interference experiment, which demonstrated the wave nature of light, sunlight was directed through a pinhole in a screen and then through two pinholes in another screen set at a considerable distance from the first screen (Jenkins & White, 1957, p. 234-235). This setup produces two spherical waves which interfere with each other and form a symmetrical intensity pattern on a third screen. The pinholes may be replaced with narrow slits in order to facilitate the use of monochromatic light instead of sunlight, which produces cylindrical wave fronts. The experiment is

perhaps best known in this form through the image of the interference fringes thus created. The geometry is similar to the one in figure 4.1 since it is assumed that the distance between the slits is much smaller than the distance to the photographic screen. (Jenkins & White, 1957, ch. 13).

The nulls of these fringes is interestingly described by equation 4.18, with the modification that D here represents the distance between the slits. Letting d denote the distance to the photographic screen, $D \sin\theta = \frac{Dx}{d}$ where x is the horizontal distance from the central fringe at the photographic screen. The fringes are therefore located at:

$$x = m\lambda\frac{d}{D} \qquad \text{(Bright fringes)} \tag{7.1}$$

$$x = \left(m + \frac{1}{2}\right)\lambda\frac{d}{D} \qquad \text{(Dark fringes)} \tag{7.2}$$

In section 4.3 it was assumed that the radiators in figure 4.1 had a constant phase difference and this applies for Young's experiment as well. If two lamps were used as sources, one in front of each slit, then no interference fringes would be observed. This is due to the fact that the light from any source will display sudden changes of phase. For visual light this change occurs in time intervals of the order of 10^{-8} seconds, and therefore the fringes cannot be maintained for longer intervals than this (Jenkins & White, 1957, p. 244). When a single monochromatic source is illuminating two slits, there is a perfect correspondence between the phase variations in the light emerging from the slits, and the phase difference is therefore constant. Regarding the slits themselves as sources, they are said to be *coherent sources*. Conversely, according to (Zernike, 1938, p. 786), *"Two vibrations of light shall be called incoherent, if their superposition gives no visible interferences"*.

While strictly monochromatic radiation is always coherent, this is not the case for radiation which has a finite spectral width. Beran and Parrent (1963, p. 29-30) distinguish between partial coherence effects due spectral spread, which they refer

to as *temporal coherence effects*, and *spatial coherence effects* which are observed for extended self-luminous sources. In Youngs' original experiment, the former appears with increasing difference in path length from the two pinholes, which causes a decay in the visibility of the fringes[1]. The time delay between the two waves are then larger than the wave's coherence time. The latter can be introduced by increasing the size of the single pinhole in the first screen, or by increasing the distance between the two pinholes in the second screen. Both of these changes will cause the visibility to decrease due to the distance between the pinholes being larger than the wave's coherence length (Beran & Parrent, 1963, p. 9-10).

In the context of SAR, the speckle phenomenon described in section 5.3 is an effect of spatial coherence. The coherence length is in this context the distance over which a target can move through the radar beam before speckle becomes significant due to the radar geometry. Time-varying target reflectivity introduces an effect of temporal coherence, with the coherence time being the time over which the target reflectivity is effectively constant.

All information regarding coherence is contained in the *mutual coherence function*, defined as:

$$\Gamma_{12}(\tau) = \langle V_1(t+\tau)V_2^*(t)\rangle \tag{7.3}$$

Here $V_1(t)$ and $V_2(t)$ represent complex field disturbances at two points P_1 and P_2, τ is a time delay, and $< \cdot >$ denotes time average. The *complex degree of coherence* is defined as:

$$\gamma_{12}(\tau) = \frac{\Gamma_{12}(\tau)}{\sqrt{\Gamma_{11}(0)\Gamma_{22}(0)}} \tag{7.4}$$

This quantity can be related to the visibility of the fringes in Young's experiment.

[1]For an illumination source with spectral width $\Delta\nu$, interference fringes are visible if the path difference Δr satisfies $\Delta r \ll \frac{c}{\Delta\nu}$

The term *visibility*[2] may be defined as:

$$\mathcal{V} = \frac{I_{max} - I_{min}}{I_{max} + I_{min}} \tag{7.5}$$

in terms of the maximum intensity I_{max} and the intensity of an adjacent minimum I_{min} (Beran & Parrent, 1963, ch. 1). The degree of coherence of two sources is by definition *"equal to the visibility of the interference fringes that may be obtained from them under the best circumstances"* (Zernike, 1938, p. 786). Hence:

$$\mathcal{V} = |\gamma_{12}(\tau)| \tag{7.6}$$

under the assumption of narrow spectral width $\Delta\nu$, i.e. $\tau\Delta\nu \ll 1$. $|\gamma_{12}(\tau)| = 0$ then represents the incoherent limit, while $|\gamma_{12}(\tau)| = 1$ is the coherent limit (Beran & Parrent, 1963, ch. 4.2).

This serves to flesh out the rather brief treatment by Elachi and van Zyl (2006, p. 30-31), who simply notes that a superposition of two (presumably real-valued) fields $E_1(t)$ and $E_2(t)$ has an average power:

$$P \propto \left\langle [E_1(t) + E_2(t)]^2 \right\rangle = \left\langle E_1(t)^2 \right\rangle + \left\langle E_2(t)^2 \right\rangle + 2 \left\langle E_1(t) E_2(t) \right\rangle \tag{7.7}$$

and that $\langle E_1(t)E_2(t)\rangle = 0$ implies that the sources are incoherent. The coherence time τ_c is defined as the time when two waves with frequencies ν and $\nu + \Delta\nu$ are out of phase by one cycle:

$$\tau_c = \frac{1}{\Delta\nu} \tag{7.8}$$

and the coherence length is defined as:

$$l_c = c\tau_c = \frac{c}{\Delta\nu} \tag{7.9}$$

which only accounts for temporal coherence. Furthermore Elachi and van Zyl define coherence simply by $\langle E_1(t)E_2(t)\rangle \neq 0$, which must necessarily also include partial

[2]Introduced by Albert Abraham Michelson in 1890 (Beran & Parrent, 1963, p. 5).

coherence. Indeed, *"Two waves are said to be coherent with each other if there is a systematic relationship between their instantaneous amplitudes"* (Elachi & van Zyl, 2006, p. 30). There is certainly some degree of coherence if the cross-covariance is non-zero. However, recalling equation 7.3, it should be noted that $\langle E_1(t)E_2(t)\rangle = \Gamma_{12}(0)$ which is of limited use by itself. For this study the quantity $|\gamma_{12}(\tau)| \equiv \rho(\tau)$ is the main quantity of interest.

7.2 System model

The model of the azimuth channel to be used in this study is the one which forms the basis for Raney (1980b), which is an extension of the model described in section 5.9. The target function $f(\eta)$ is now modulated by a stochastic process $\{\alpha(\eta|x)\}$, where $\{\cdot\}$ shall be used as notation for a stochastic process. The target coherence is dependent on on how fast the autocorrelation function of $\{\alpha\}$ decays. In the non-coherent limit all samples are independent. The block diagram for this system model is shown in figure 7.1.

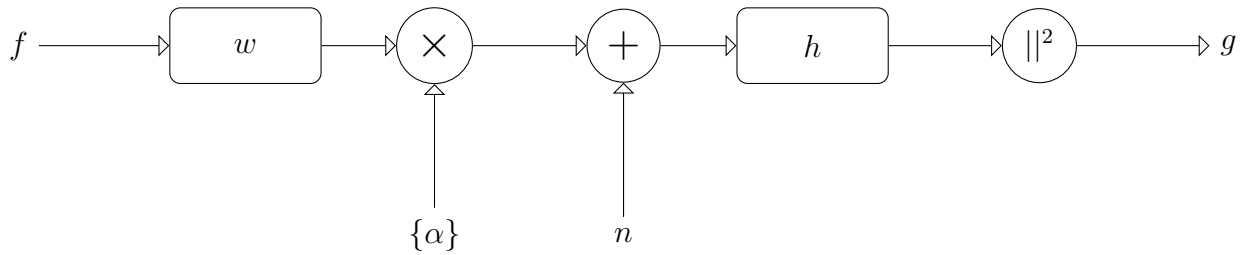

Figure 7.1: Block diagram describing a model of the SAR azimuth channel where partial temporal coherence has been introduced. Comparing with figure 5.6, the scene input function is now modified by a random phase shift $\{\alpha(\eta)\}$, where $\{\cdot\}$ is used to denote a stochastic process. Based on figure 5c in Vachon (1983).

The target function $f(\eta)$ is commonly also be described as a stochastic process due to the speckle phenomenon described in section 5.3. However, in order to separate the effects caused by the temporal coherence it is convenient to neglect speckle noise, which is a valid approach under the assumption that only targets with a coherence

length longer than the footprint are considered.

The justification for multiplying α with the output of the prefilter is the observation that α is conditional, but not dependent, on the position of the corresponding scene element (Raney, 1980a, p. 36). In simulating this model the multiplication is straightforward for a single point target since each return is associated with only one scattering element. However, in the case of an extended scene the spatial dependence most be handled correctly, as shall be discussed in chapter 9.

The explicit expression for the azimuth prefilter provided by Raney (1980b, p. 778) relies on the rectilinear approximation which was mentioned in section 5.7. The change of variables $x = V_r\eta$ is introduced, and the prefilter takes the form[3]:

$$w(x) = w_a(x)\, e^{-i\frac{2\pi}{\lambda R_0}x^2} \tag{7.10}$$

This is consistent with equation 5.47 and equation 5.30 for the zero-squint case, where the quantities involved are related by:

$$\frac{B_D}{T_a} = \frac{2V_r^2}{\lambda R_0} \tag{7.11}$$

which is the FM rate of change of the Doppler chirp, here set to be positive. The factor $w_a(x)$ is the weighting of the far field due to the azimuth antenna pattern, for which a Gaussian function is used:

$$w_a(x) = e^{-\frac{ax^2}{2}} \tag{7.12}$$

This is a good approximation to the main lobe of equation 5.18 within the FWHP beamwidth for an appropriate value of a, which is determined by calculating the

[3]Raney (1980a, 1980b) starts out with a positive exponent in equation 7.10 and ends up with a negative one midway through the derivations. For consistency a negative exponent is here introduced from the start, in line with the argument given in section 5.5.

equivalent rectangle[4] of $w_a(x)$:

$$\int \frac{w_a(x)}{w_a(0)} dx = \int e^{-ax^2}\, dx = \sqrt{\frac{2\pi}{a}} \int \sqrt{\frac{a}{2\pi}} e^{-ax^2}\, dx = \sqrt{\frac{2\pi}{a}} \tag{7.13}$$

since the last integral is a Gaussian probability density function with variance a^{-1}. This is a measure of half the azimuth footprint, which is equal to $R\beta_a$ by the small angle approximation $\tan(\beta_a) \approx \beta_a$, β_a being the azimuth beamwidth. Hence a can be determined by:

$$\sqrt{\frac{2\pi}{a}} = R\beta_a \quad \Longrightarrow \quad a = \frac{2\pi}{(R\beta_a)^2} \tag{7.14}$$

[4]The equivalent rectangle of a complex filter $h(t)$ can be defined as $\int \frac{|h(t)|}{|h(t_0)|}\, dt$ or $\int \frac{|h(t)|^2}{|h(t_0)|^2}\, dt$, where $|h(t_0)|$ is the peak value of $|h(t)|$. The idea is to obtain the width of a rectangle having the same area and maximum height as the (squared) norm of $h(t)$ (Brown, 1963, p. 149).

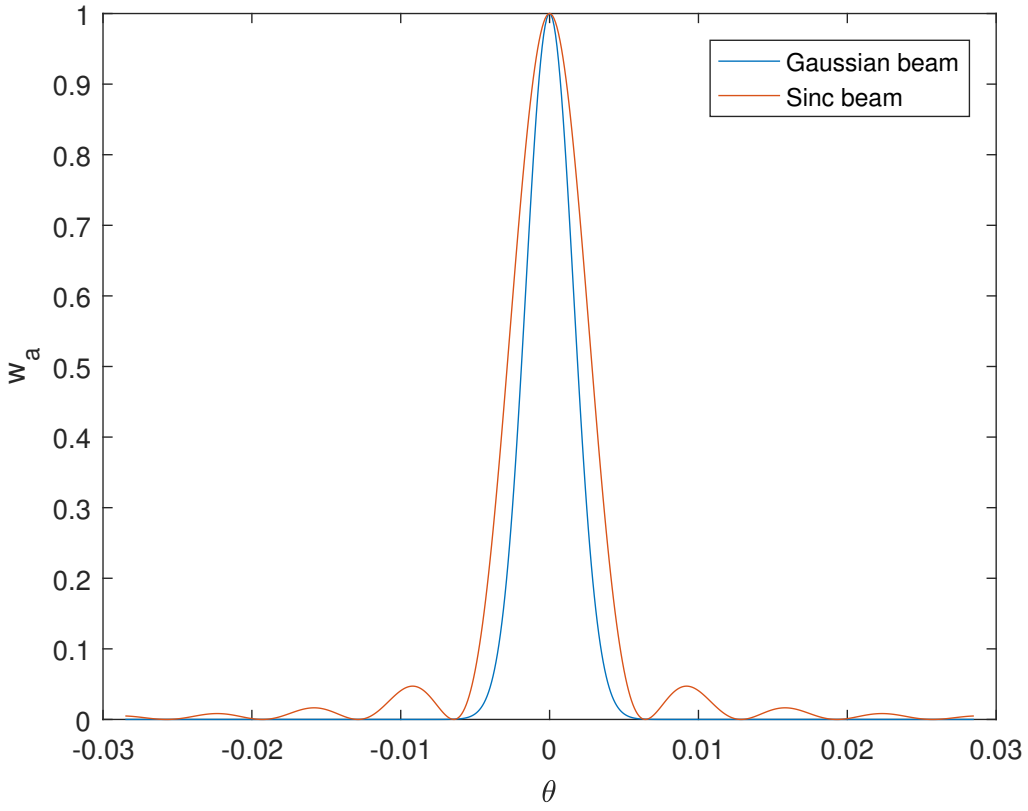

Figure 7.2: Comparison of the antenna patterns given by equation 5.18 (red) and equation 7.12 (blue) for the radar parameters in table 8.1.

Following the notation in Raney (1980b), let:

$$b = \frac{4\pi}{\lambda R_0} \tag{7.15}$$

and:

$$c = \frac{a}{2} + i\frac{b}{2} \tag{7.16}$$

The prefilter is then expressed as:

$$w(x) = e^{-cx^2} \tag{7.17}$$

and the matched filter is given by:

$$h(x) = w^*(-x) = w^*(x) \tag{7.18}$$

where the last equality is due to the quadratic dependence on η.

The stochastic process $\{\alpha(\eta|x)\}$ is assumed to be wide-sense stationary with a Gaussian autocorrelation function which takes the form:

$$\rho(\tau) = e^{-\pi \frac{\tau^2}{\tau_c^2}} \tag{7.19}$$

where τ denotes time lags and τ_c is the correlation time, which is defined by this expression. The factor π which appears in the exponent seems to be an arbitrary choice, and does not appear in e.g. Carande (1994), who reports the results of measuring ocean coherence time under the assumption of a Gaussian autocorrelation function.

Changing variables to $u = \tau V_r$, ρ can be written as:

$$\rho(u) = e^{-\frac{\pi u^2}{(\tau_c V_r)^2}} \equiv e^{-\frac{B}{2}u^2} \tag{7.20}$$

where, still in keeping with the notation in Raney (1980b), $B \equiv \frac{2\pi}{(V_r \tau_c)^2}$.

7.3 Partially coherent quadratic filtering

Recalling the quadratic filter defined in section 6.1 and the expression of $w(\eta)$ given in the previous section, the quadratic filter of a partially coherent SAR processor is, according to Raney (1980b, p. 778) given by:

$$Q(x, y) = \gamma(y - x)\, w^*(-x)\, w(-y) \tag{7.21}$$

where γ is a correlation function, here chosen by Raney to be a Gaussian function:

$$\gamma(u) = e^{-\frac{A}{2}u^2} \tag{7.22}$$

which has exactly the same form as equation 7.20. Hence:

$$Q(x,y) = e^{-\frac{A}{2}(y-x)^2}\, e^{-c^* x^2}\, e^{-cy^2} \tag{7.23}$$

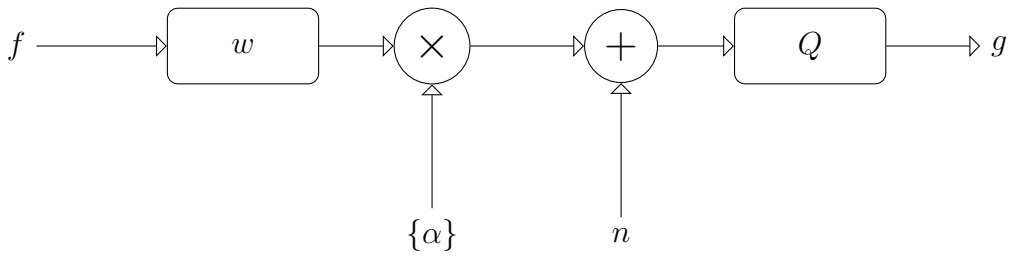

Figure 7.3: Modification of the block diagram in figure 7.1. The filter h and magnitude squared operation has here been replaced with a quadratic filter.

Raney provides a number of results based on the explicit forms of w and ρ given in the previous section.

- If the coherence time of the scene is known, then setting $A = B$ maximizes the ratio (expected signal)^2/(noise variance). Assuming $B \gg a$, this degrades the resolution by a factor $\sqrt{2}$ beyond the scene limited quantity[5] (Raney, 1969b, as cited in Raney, (1980a, p. 39)). This result, which is crucial for motivating this thesis, seems to be available in Raney (1969b) only. Raney's dissertation has proven to be hard to locate, and the result must therefore be taken on faith alone.

- Setting $A > 0$ the aperture is restricted during processing. Let the fraction of the restricted aperture and the total available aperture be denoted by n^{-1}. Then $A = n^2 a$, and the number of independent looks N is given by:

$$N = \sqrt{1 + n^2} \tag{7.24}$$

[5]This term, used by Raney (1980b, p. 780), is not explained in Raney's articles, but presumably refers to the highest resolution that can be achieved by the SAR system in the presence of partial coherence in the scene.

- The expected impulse response of a point target located at $x = 0$ is[6]:

$$E[g_\delta(u)] = \iint Q(u-x, u-y)w(x)w^*(y)\rho(y-x)\,dx\,dy \tag{7.25}$$

If $A = B$ the contributions from scene and processor partial coherence is collected in a factor $\rho(y-x)^2$, the rest being equal to equation 6.1 with $u = V_r\eta$.

- Under the assumption of a large TBP and the explicit formulas given for the quantities involved, the resolution of a partially coherent SAR is given by:

$$\delta_a = \frac{\sqrt{2\pi(A+B+a)}}{b} \tag{7.26}$$

In the coherent limit this is equal to half the antenna length. This resolution happens to be the reciprocal of the image bandwidth for a sinusoidal wave field:

$$f(x;t) = \sqrt{\sigma_B}\alpha(t|x)\,(1 + m\,\cos\omega x) \tag{7.27}$$

where m is a modulation index on the mean reflected amplitude σ_B. The modulation $\alpha(t|x)$ here represents capillary waves.

- The Fourier transform of the impulse response of the whole SAR system, including the prefilter, can be obtained by augmentation and association of variables. This is given by:

$$\tilde{g}_\delta(\omega) = \gamma\left(\frac{\omega}{b}\right)\rho\left(\frac{\omega}{b}\right)\frac{1}{2\pi}\int \tilde{h}(\omega-\lambda)\tilde{w}(\omega-\lambda)\tilde{h}^*(-\lambda)\tilde{w}^*(-\lambda)\,d\lambda \tag{7.28}$$

under the assumption of a large TBP (Raney, 1981a, p. 743). Taking the inverse Fourier transform of this expression should in principle yield a one-dimensional impulse response where the correlation structure is still preserved, although it

[6]Raney (1980a) includes a power factor σ in the impulse response. Here it is assumed that the input to the azimuth prefilter is an impulse, and this factor is therefore omitted without loss of generality since it can be multiplied back in at any stage.

was introduced through augmentation of variables. The derivation of this result is the topic of Raney (1981b), a summary of which is presented in appendix B.

- For a deterministic real-valued input $f(x)$ it is possible to derive a transfer function for the whole SAR system, including the prefilter, through augmentation and association of variables. Let $F(x) \equiv f(x)^2$. Then:

$$\tilde{g}(\omega) = \tilde{F}(\omega)\tilde{g}_\delta(\omega) \tag{7.29}$$

with $\tilde{g}_\delta(\omega)$ defined above.

The question of dependence between partial coherence and expected quantities is covered in depth by Raney and seems to be the main topic of the discussion in these articles. In summary:

- The integral over the impulse response under the assumption of large TBP is independent of scene and system coherence. Hence a SAR with large TBP is energy conservative. This has an analog when considering the expected output due to partially scene coherence, namely that the effective gain of the SAR is also independent of scene and system coherence.

- The expected output in the presence of receiver noise alone is independent on system coherence, while the noise variance is a function of system coherence, as is the effective noise bandwidth, both decreasing with coherence decreases.

- The mean output signal for a distributed scene is independent of scene and system coherence, while the signal output variance decreases as partial system coherence is introduced.

- The variance to mean-squared ratio of a SAR observing a partially coherent scene decreases with system coherence, but is independent of scene coherence.

- The bandwidth of the SAR including the azimuth prefilter decreases as system coherence is reduced.

Finally, one crucial observation is that ρ and τ_c are, in practice, not measurable from SAR data (Raney, 1980b, p. 786). Furthermore, *"no evidence of degraded resolution (for a distributed scene) is available in the image"* (Raney, 1980b, p. 786).

7.4 Discussion

So far the the aspects of SAR theory which relates to the articles by Raney have been discussed in order to understand the basis and limitations of the proposed method.

The essence of partially coherent processing is the factor $\gamma(y - x)$ in equation 7.21. This factor is assumed to be a correlation function. For a scene function $f(x)\alpha(t|x)$, setting γ equal to the autocorrelation function of α maximizes the expected signal squared to noise variance ratio at a cost of decreased resolution. This approach relies on the introduction of a second variable since the γ factor introduces a coupling between the two independent variables x and y.

Figure 6.1 presents a scheme for transforming the non-linear quadratic filter formulation into an LTI system by an operation referred to as augmentation of variables. Filtering can either be done in the time domain by setting $g(u) = G(u, u)$ after filtering, or by following the scheme clockwise and filtering in the frequency domain. The formalism has been completely rederived and is found to be formally correct. Therefore, the results in Raney's articles may also be considered formally correct. The decoupling of the range and azimuth directions is also valid, as described in section 5.9. It is assumed that range cell migration has been perfectly corrected. The Gaussian antenna pattern of equation 7.12 is also a good approximation to the sinc pattern of equation 5.18, as illustrated in figure 7.2.

The optimal processor coherence is governed by the scene coherence time, which cannot be extracted from the SAR data and must therefore be determined by other means (e.g. Carande (1994) or Shemer and Marom (1993) in the case of ocean

coherence time). The factor π that appears in the autocorrelation function (equation 7.20) seems to be an arbitrary scaling and can be neglected. While Raney considers an arbitrary stationary process $\{\alpha\}$ (presumably for convenience in order to derive closed-form expressions) Raney (1981a) and Vachon (1983, p. 20) define a partially coherent target as one that undergoes a phase modulation $e^{i\{\theta\}}$. While this prevents analytical development in terms of the coherence time of $\{\theta\}$, it links the coherence time with the phase error, which is the physically observable quantity. The choice of $\{\alpha\}$ leaves much freedom in modelling, and for simplicity the definition of Vachon shall be used to restrict the partial scene coherence to a random phase fluctuation. Therefore τ_c shall henceforth denote the coherence time of $\{\theta\}$.

Chapter 8

Point target simulation

The most central aspects of SAR theory which are relevant to Raney's quadratic filter formulation have now been covered, and based on this the formulation itself seems to be sound. The next step is to generate some simulated data in order to study the effect of processing partially coherent targets using this approach. This chapter shall restrict itself to partially coherent point targets, and based on these results some remarks on the obtainable resolution shall be made.

8.1 Implementation

The following describes an implementation of the model in chapter 7, specifically figure 7.1 and figure 7.3. From the definitions of a and b, the radar parameters required are the radar altitude R_0, radar velocity V_r, radar wavlength λ and beamwidth β. The latter depends on λ and antenna length L_a. Recalling the expression for the the first null beamwidth in section 4.3, let:

$$\beta_a = \frac{\lambda}{L_a} \tag{8.1}$$

The last quantity involved is the sampling period T_s which is the reciprocal of the pulse repetition frequency (PRF). The radar parameters used in the subsequent modelling is described in table 8.1.

R_0	Radar altitude	800 km
V_r	Effective radar velocity	7100 m/s
λ	Radar wavelength	0.057 m
L_a	Antenna length	10 m
f_s	Azimuth sampling rate (PRF)	1700 Hz

Table 8.1: Radar parameters from table 4.1 in Cumming and Wong (2003).

The radar footprint in units of length along the azimuth axis is equal to $2R_0 \tan \beta_a$, and the exposure time is therefore:

$$T_a = 2\frac{R_0 \tan \beta_a}{V_r} \equiv 2\eta_0 \tag{8.2}$$

which in this case is approximately 1.28 s. Suppose that a target enters the beam at $-\eta_0$, and exits at η_0, with $\eta = 0$ corresponding to the time at which the radar passes directly over the target. The azimuth prefilter is then implemented as equation 7.17:

$$w(\eta) = e^{-cV_r^2\eta^2} \tag{8.3}$$

evaluated at times $[-\eta_0, \eta_0]$ with a spacing T_s.

Once the target vector is convolved with the prefilter vector, the result is multiplied with the random vector $e^{i\theta}$ where θ is a sample from a random Gaussian process with a correlation time τ_c.

The generation of the sample θ is not trivial, and shall be discussed further below. The additive noise can be modelled as a white Gaussian complex process:

$$n \sim \sigma_n(N(0,1) + iN(0,1)) \tag{8.4}$$

where σ_n is the noise standard deviation. This shall be set to 0.25 times the maximum amplitude of the signal in the following simulations. Once this has been added to the

signal, the result can be convolved with the matched filter h which is simply the complex conjugate of w. This is the coherent processing normally used when compressing SAR data. The output should be divided by the power of the filter and calibrated so that the image represents the radar backscatter coefficient σ^0 as given in equation 5.6.

The scaling of the output is not of great interest in the study of target coherence, but rather the shape of the resulting signal. Therefore the maximum amplitude of the target vector, which is equal to the square root of the power at the sensor might as well be set to 1, so that σ_n can be adjusted accordingly to yield the desired SNR.

8.1.1 Generation of correlated Gaussian random numbers

Deserno (2002) describes a method for generating correlated Gaussian random numbers r_n with zero mean and unit variance.

Starting with a sample g_n, define the correlation coefficient:

$$f \equiv e^{-\frac{1}{|\tau|}} \tag{8.5}$$

where τ is the number of lags over which r_n is coherent. Next define the sequence r_n by te recursive relation:

$$\begin{aligned} r_0 &\equiv g_0 \\ r_n &\equiv f\, r_n + \sqrt{1-f^2} g_{n+1} \end{aligned} \tag{8.6}$$

or equivalently:

$$r_n = f^n g_0 + \sqrt{1-f^2} \sum_{i=1}^{n} g_i f^{n-i} \tag{8.7}$$

By induction:

$$\begin{aligned} E[r_{n+1}] &= fE[r_n] + \sqrt{1-f^2}E[g_{n+1}] = 0 \\ E[r_{n+1}^2] &= f^2E[r_n^2] + (1-f^2)E[g_{n+1}^2] = 1 \end{aligned} \tag{8.8}$$

and the autocorrelation function is:

$$\begin{aligned} \rho[n] &= E[r_m r_{m+n}] \\ &= E\left[r_m\left(f^n r_m + \sqrt{1-f^2}\sum_{i=m+1}^{m+n} g_i f^{m+n-i}\right)\right] \\ &= f^n E\left[r_m^2\right] \\ &= e^{-\frac{n}{|\tau|}} \end{aligned} \tag{8.9}$$

where the second equality is due to the fact that r_m is not correlated with g_i for $i > m$.

Although this procedure yields an exponential decay in the autocorrelation function, the assumption of ρ having a Gaussian shape can be considered one of convenience and not a necessary condition since the exponential decay does not alter the physical interpretation of the coherence time.

In the case of a point target there is no summation involved in each step in the convolution between the target function and the prefilter. Hence the output of the prefilter can be multiplied directly with the random vector $\{\alpha\}$ in order to model partial scene coherence. For an extended scene the process is rather more involved since the convolution must keep track of azimuth time as well as the time dependence of the random phase fluctuation. This shall be explored in the next chapter.

8.1.2 Implementation of the quadratic filter

The obvious method of implementing the quadratic filter in MATLAB is to define space vectors $x = y = V_r\eta$, where η is the vector used to construct the azimuth prefilter, and then define a meshgrid `[X,Y] = meshgrid(x,y)` and plug `X` and `Y` into the definition of Q, thereby forming a complex-valued image. Recalling that:

$$g(u) = \iint Q(u-x, u-y)\, w(x) w^*(y)\, dx\, dy \tag{8.10}$$

Define the image $w(x)w^*(y) \equiv W(x,y)$ and augment variables to:

$$G(u,v) = \iint Q(u-x, v-y)\, W(x,y)\, dx\, dy \tag{8.11}$$

which is a 2D convolution integral. The filtering can then be done by the `conv2` function, which is somewhat computationally inefficient. Instead `Q` and `W` can be zero-padded to twice the size of `W`, after which the fast Fourier transform `fft2` is applied to both images, the result of which is multiplied element-wise. By the convolution theorem this is equivalent to a convolution. The inverse fft can then be applied, and the padding removed by cropping the image. The main diagonal then corresponds to $u = v$, which is the desired result.

Figure 8.1 shows plots of $|Q|$ for different values of A, which illustrates how partial processor coherence affects the envelope of the quadratic filter. It may be noted that the main diagonal remains unaffected.

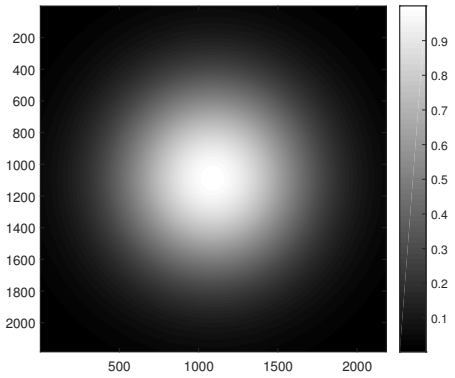

(a) $A = 0$

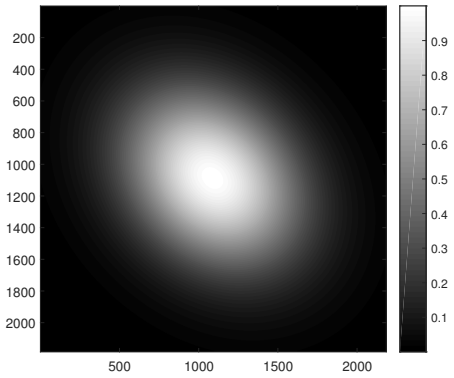

(b) $A = 10^{-7}$

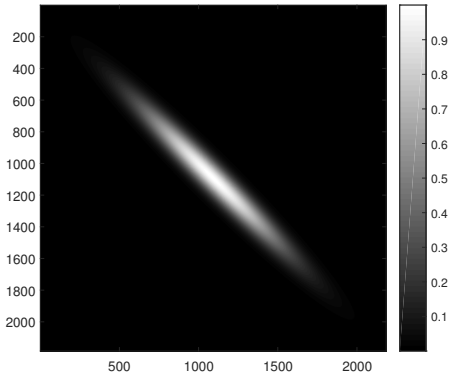

(c) $A = 10^{-5}$

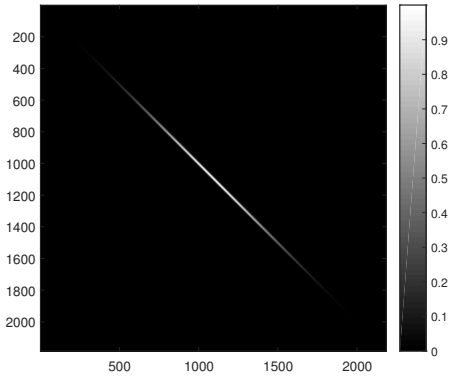

(d) $A = 10^{-3}$

Figure 8.1: Comparison of $|Q|$ for different values of A.

In order to set the optimal processor coherence, it is necessary to know the coherence time of the scene. Since $\{\alpha\} = e^{i\pi\{\theta\}}$ and the coherence time of $\{\theta\}$ is chosen, the coherence time of $\{\alpha\}$ is required due to the formulation of Raney. As already stated, the coherence time shall be defined as the time it takes for the autocorrelation function to decay by a factor $e^{-1} \approx 0.4$. Since calculating the autocorrelation function of $\{\alpha\}$ given the coherence time of $\{\theta\}$ proves rather intractable, it shall be taken as a rule of thumb that the coherence time of $\{\alpha\}$ is approximately one tenth of the coherence time of $\{\theta\}$. This may be justified by comparing the autocorrelation plots of the respective processes, which is shown in figure 8.2. Hence an approximation to the

optimal processor coherence time is:

$$B = \frac{2}{(\frac{\tau_c}{10} V_r)^2} \tag{8.12}$$

which, as shall be demonstrated, is sufficiently accurate for the present purposes.

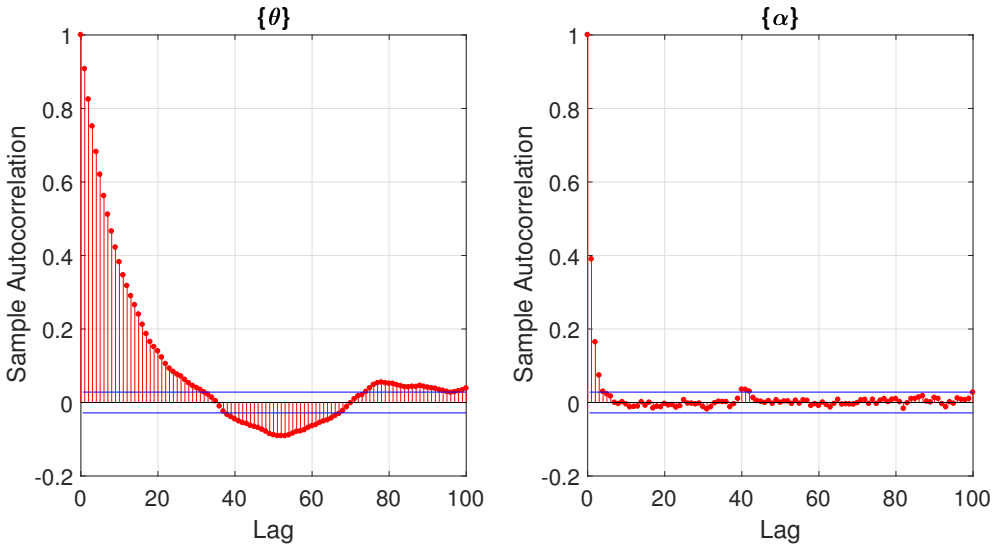

(a) Estimated autocorrelation functions for $\{\theta\}$ (left) and $\{\alpha\} \equiv e^{i\pi\{\theta\}}$ (right) given that $\{\theta\}$ is coherent over 10 lags.

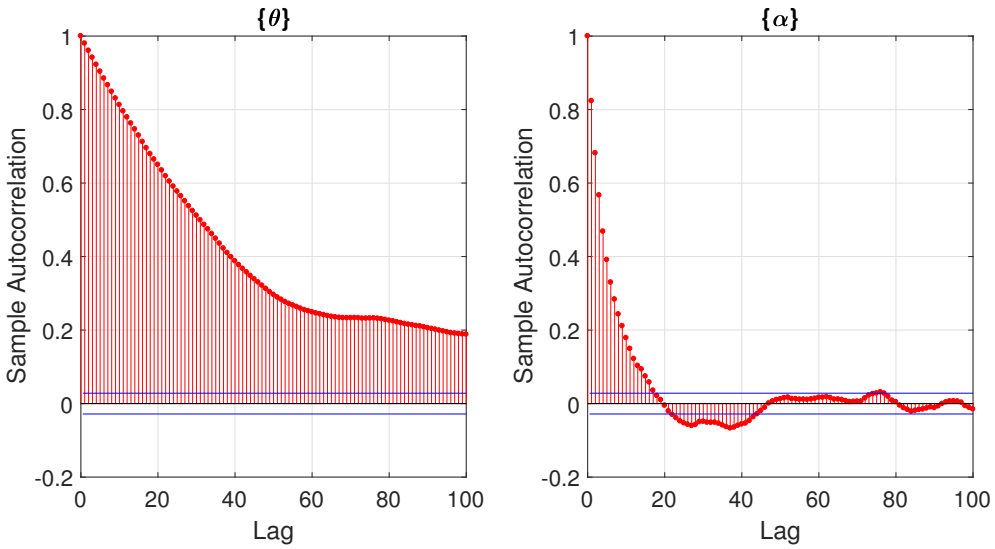

(b) Estimated autocorrelation functions for $\{\theta\}$ (left) and $\{\alpha\} \equiv e^{i\pi\{\theta\}}$ (right) given that $\{\theta\}$ is coherent over 50 lags.

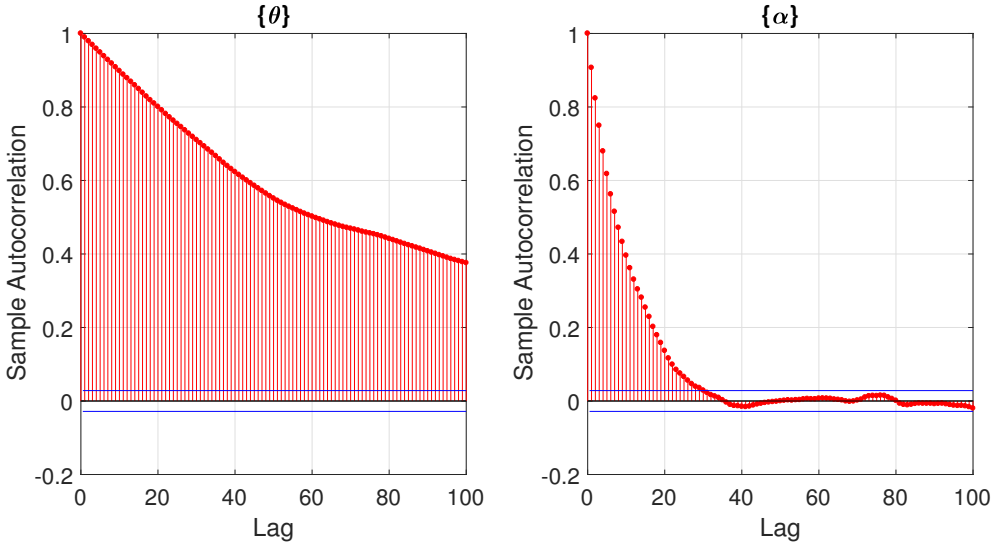

(c) Estimated autocorrelation functions for $\{\theta\}$ (left) and $\{\alpha\} \equiv e^{i\pi\{\theta\}}$ (right) given that $\{\theta\}$ is coherent over 100 lags.

Figure 8.2: Comparison of estimates of the autocorrelation functions of $\{\theta\}$ (left column) and $\{\alpha\} \equiv e^{i\pi\{\theta\}}$ (right column) for different number of lags over which $\{\theta\}$ is coherent. The blue lines show the confidence bounds of two standard errors.

8.2 Results

Figure 8.3 illustrates how a point target behaves as partial coherence is introduced in the scene. Once the coherence time becomes smaller than the integration time of the SAR, the point target loses strength while the resolution is slightly degraded. At coherence times much smaller than the integration time the target is hardly visible. Figure 8.4 shows the same results using a quadratic filter with $A = 0$, from which it can be verified that the quadratic filter formulation is valid in the case of coherent processing.

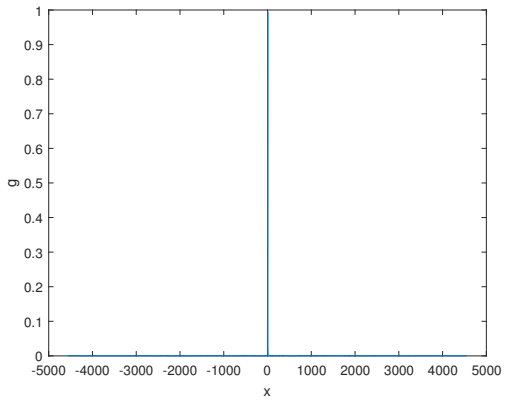

(a) $\tau_c = \infty$ s

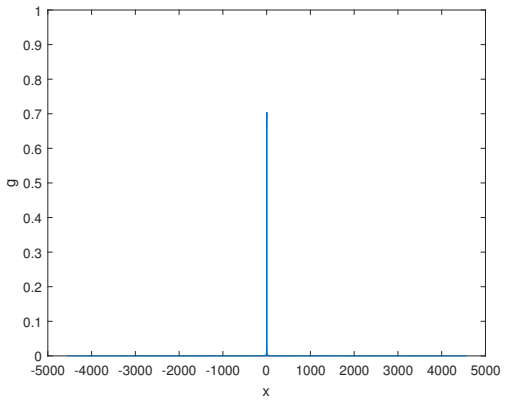

(b) $\tau_c = 10$ s

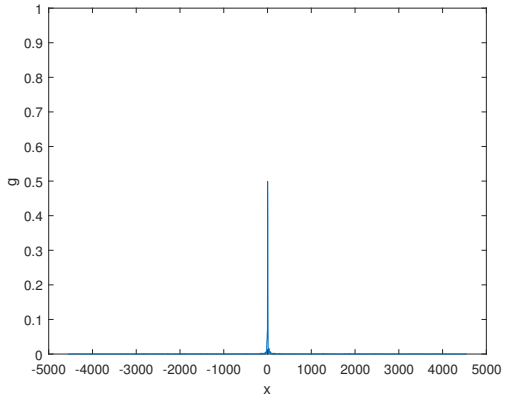

(c) $\tau_c = 1$ s

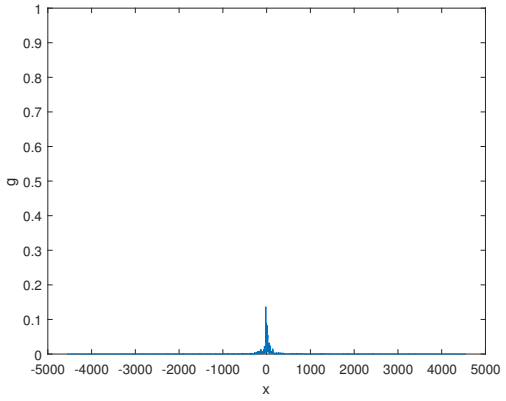

(d) $\tau_c = 0.1$ s

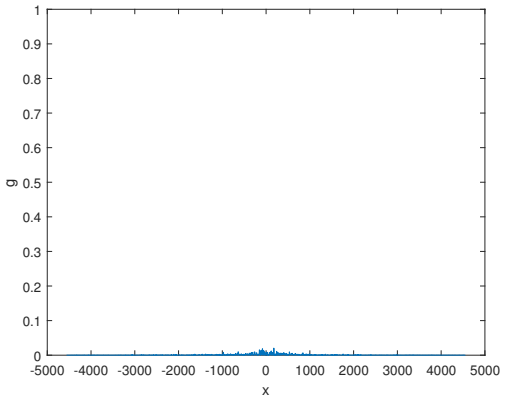

(e) $\tau_c = 0.01$ s

Figure 8.3: Comparison of point target response for various coherence times using a 1D matched filter. The target becomes less visible as the coherence decreases, as predicted by the theory.

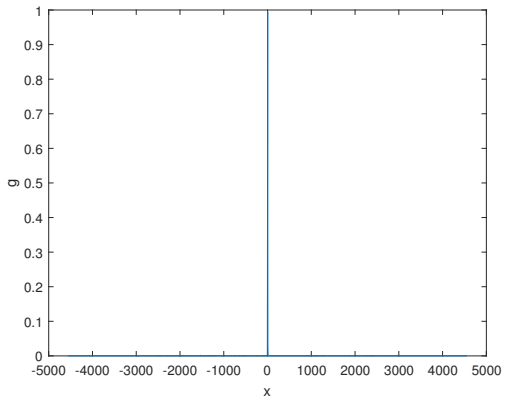

(a) $\tau_c = \infty$ s

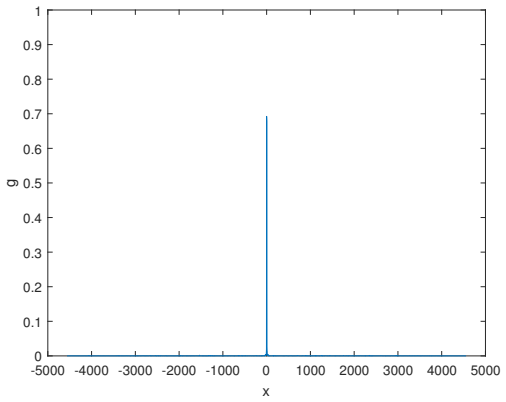

(b) $\tau_c = 10$ s

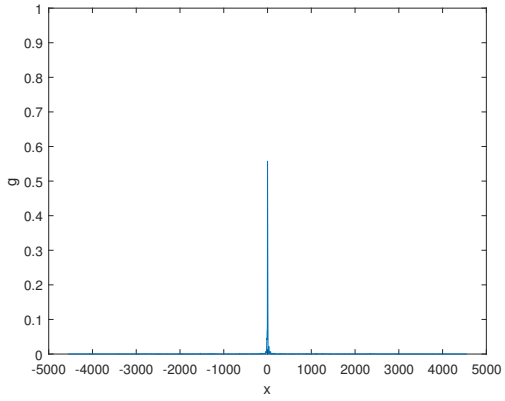

(c) $\tau_c = 1$ s

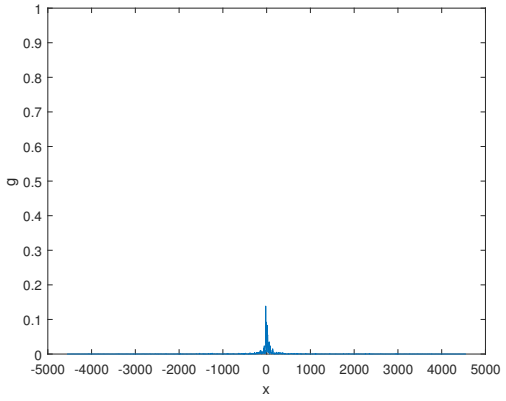

(d) $\tau_c = 0.1$ s

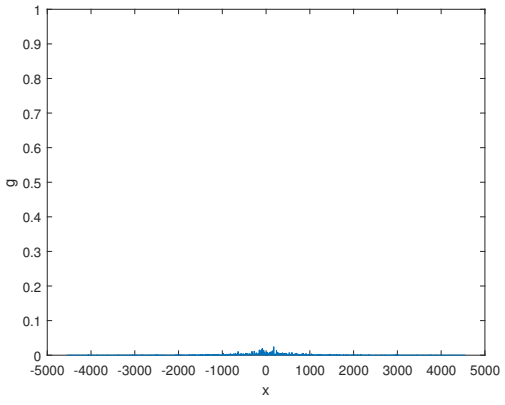

(e) $\tau_c = 0.01$ s

Figure 8.4: Comparison of point target response for various coherence times using a coherent quadratic filter. Comparing these results with the ones in figure 8.3, it can be verified that a fully coherent quadratic filter produces the same results as a standard 1D matched filter.

Consider the case of $\tau_c = 0.5$. Figure 8.4 illustrates the effect of introducing partial coherence in the processor as well. A further decrease in amplitude is observed while the shape of the output is smoother. The optimal case of $A = B$, shown in figure 8.5c, should according to Raney maximize the ratio (expected signal)^2/(noise variance), as discussed in section 7.3.

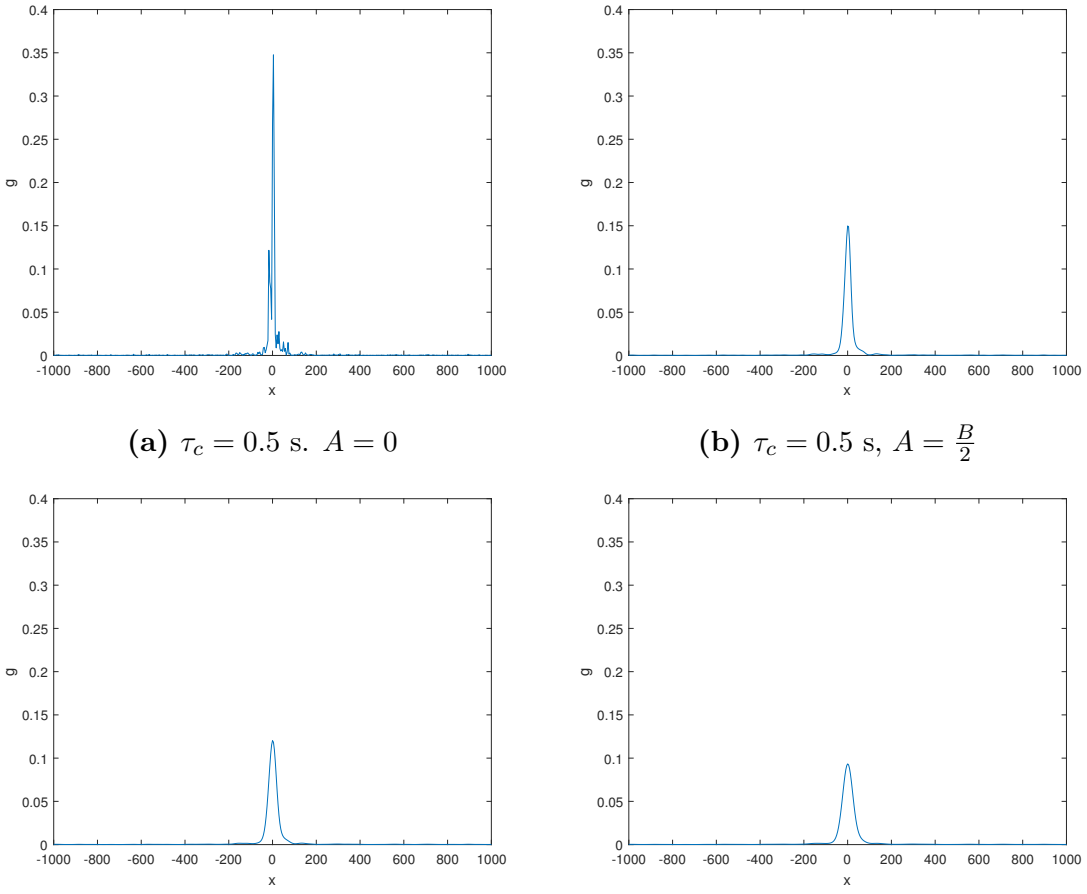

(a) $\tau_c = 0.5$ s. $A = 0$

(b) $\tau_c = 0.5$ s, $A = \frac{B}{2}$

(c) $\tau_c = 0.5$ s, $A = B$

(d) $\tau_c = 0.5$ s, $A = 2B$

Figure 8.5: Comparison of point target response for various coherence times using a partially coherent quadratic filter.

Recalling equation 7.26, the theory predicts a resolution of approximately 63 m in the optimal case. Figure 8.6 relates this number to the half power width of the target response, which is roughly 40 m in this case. As noted in section 4.3, this is one

possible measure of resolution. Considering the margin of error in the estimation of the coherence time of $\{\alpha\}$, as well as the fact that this number is based on the expected impulse response, this correspondence may be considered satisfactory. Compared to the optimal coherent case of 5 m given by equation 5.40, the degradation in resolution is significant. While the reduction in resolution was predicted by the theory, the reduction in amplitude shown in figure 8.5 is inconvenient for the purpose of target detection. It may therefore seem that the criterion of maximizing the ratio (expected signal)^2/(noise variance) may be of limited use for this purpose.

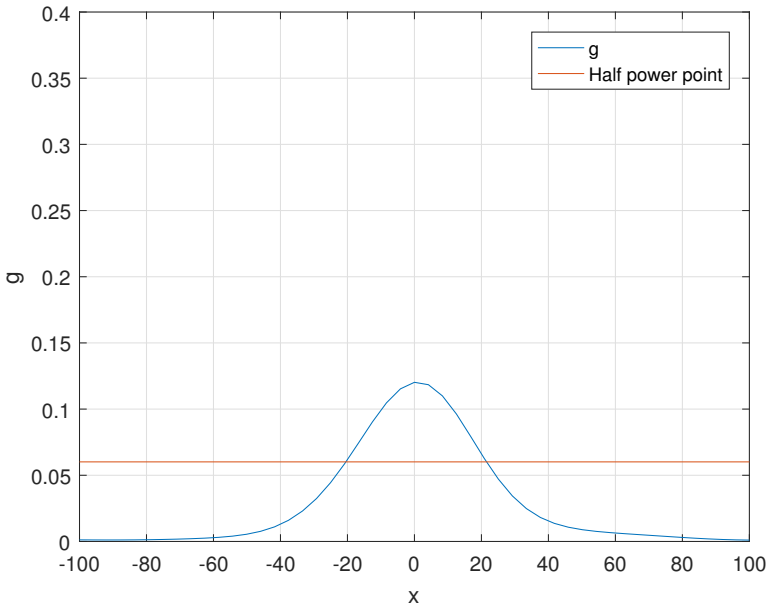

Figure 8.6: Illustration of the half power width of the point target response for $\tau_c = 0.5$ s and $A = B$. The half power width, which here is roughly 40 m, is one possible measure of resolution and can be compared with the resolution predicted by equation 7.26, which is 63 m. The optimal resolution is 5 m as given by equation 5.40. The degradation in resolution predicted by the theory is roughly in agreement with the one obtained in the simulation .

Chapter 9

Distributed scene simulation

Having simulated a point target, this chapter deals with case of a point target embedded in a distributed scene. Suppose that a point target is surrounded by a number of weaker scatterers with a significantly shorter coherence time. The question is whether or not it is possible to use Raney's formalism in order to strengthen the response of the more coherent point target.

9.1 Motivation

The weighting of the quadratic filter in Raney's articles has a Gaussian shape due to the assumption of the shape of the autocorrelation function. If the response of the point target and the background of the scene combined is considered as a superposition of the two, then it is reasonable to suspect that there is something to gain by setting:

$$\gamma(u) \equiv e^{-\frac{A_{target}}{2}u^2} - e^{-\frac{A_{background}}{2}u^2} \tag{9.1}$$

Intuitively, this scooping of the envelope of this quadratic filter, henceforth referred to as a scooped filter, should strengthen the signal from the point target by limiting the integration such that the return from the background is mostly excluded. The case of interest in the following sections is when the point target has a coherence time

an order of magnitude above the scene.

9.2 Implementation

As already mentioned, a distributed scene requires a separate implementation of the convolution between the scene function and the azimuth prefilter where the random phase fluctuation is applied in each convolution step according to the procedure described in section 8.1.1. This has been achieved by manually implementing the convolution in the usual way by a for-loop. During a regular discrete convolution process the flipped azimuth prefilter slides over the target vector, and at each step the overlapping elements of the two vectors are multiplied, and the products summed in order to produce one element in the convolution vector (MathWorks, n.d.).

The modification consists of forming a matrix of column vectors, each of which is a realization of the $\{\alpha\}$-process with a chosen coherence time, and weighting the sum of each convolution step by the appropriate vector picked out from the random matrix. In this way each element of the scene is weighted by an element from its corresponding column in the random matrix at each step in the convolution, and as the convolution progresses the weight evolves according to the imposed temporal correlation.

The background has been modelled using the same procedure from section 8.1.1. A Gaussian random vector is first formed, and the correlation structure is then applied to this random vector. Thus a spatial correlation has been introduced as well, which accounts for the speckle phenomenon discussed in section 5.3.

9.3 Results

Consider the case where $\tau_{c,background} = 0.0588$ s, $\tau_{c,target} = 0.588$ s and the spatial coherence length l_c is 208.8 m. The envelope of the corresponding quadratic filter is illustrated in figure 9.1.

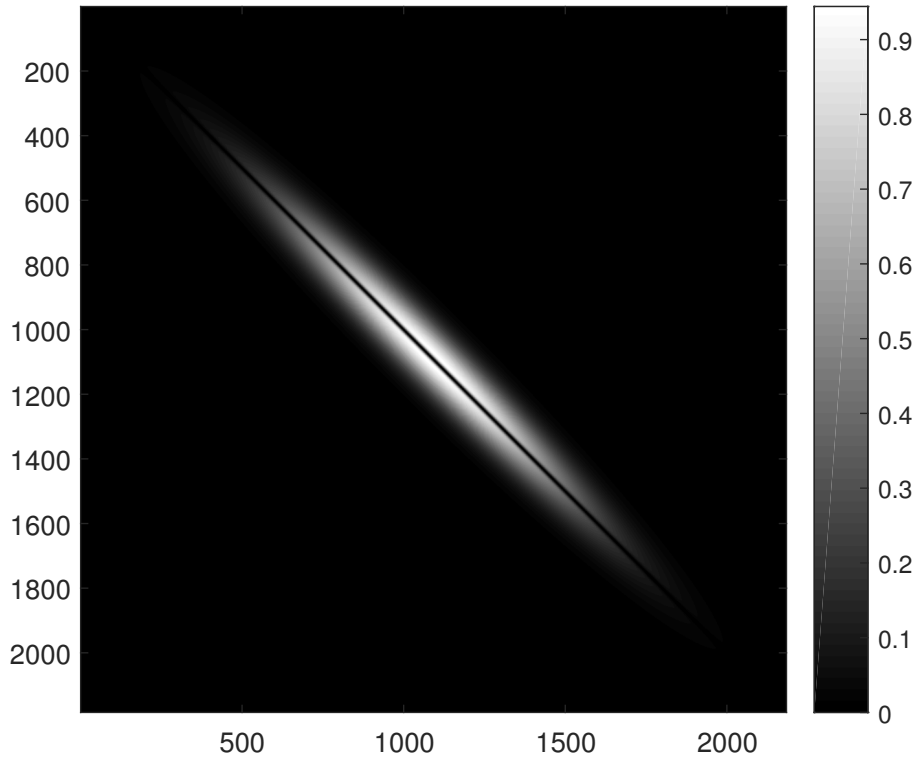

Figure 9.1: Plot of the scooped quadratic filter envelope for $\tau_{c,background} = 0.0588$ s and $\tau_{c,target} = 0.588$ s.

The background variance is constant and set to 1, and the power of the point target at the sensor has been set to 10. A scene of 2088 m has been modelled, and it is assumed that the surrounding reflectivity is zero. The scene has been processed using a 1D matched filter, to which has been applied a 10 point running average filter, and a quadratic filter with a scooped envelope. The coherence of the quadratic filter has been set to optimum. The result is shown in figure 9.1.

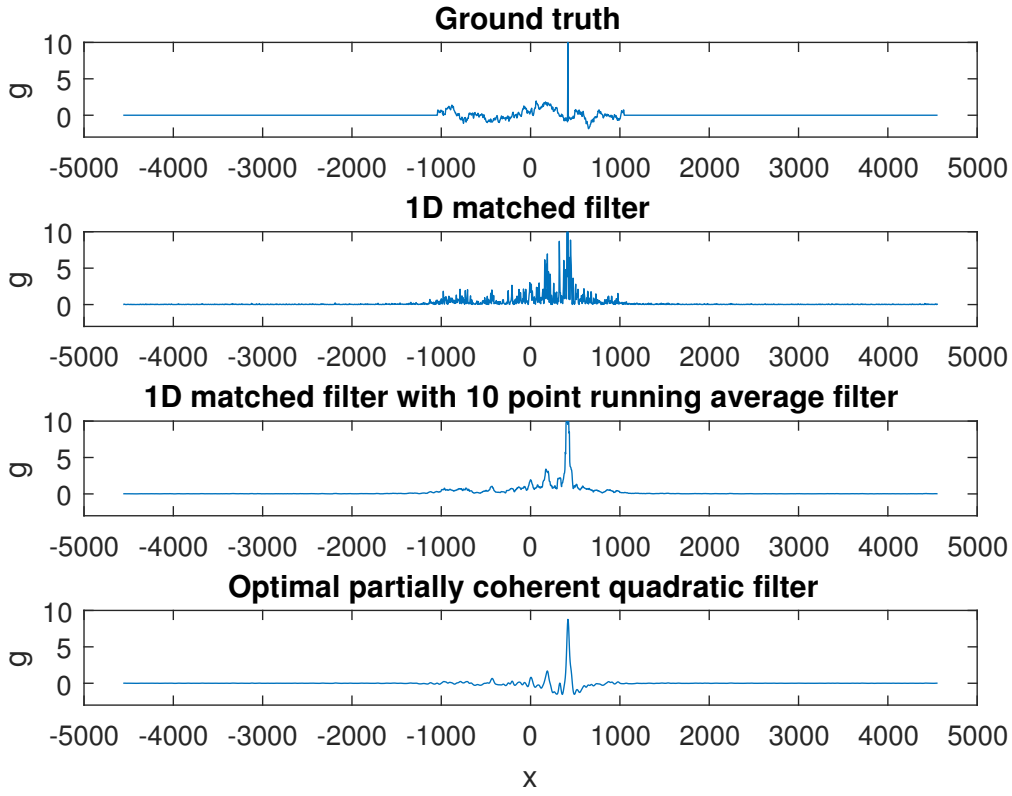

Figure 9.2: Distributed scene simulation 1. $P_r = 10$, $l_c = 208.8$ m, $\tau_{c,background} = 0.0588$ s, $\tau_{c,target} = 0.588$ s.

It is interesting to note that the quadratic filter produces slightly negative values. This is not surprising since the quadratic filter is no longer necessarily a correlation function according to the requirements stated in section 6.2. Specifically, the filter Q which is used here is not necessarily positive definite since it is now a difference between two Gaussian functions. A slight relaxation of the requirements for a quadratic filter described in chapter 6 has therefore been introduced. Apart from this, it is similar to the averaged output of the 1D matched filter. The point target emerges quite strongly from the background.

Suppose that the power of the point target is reduced from 10 to 5. In this case it is

hardly detectable, as shown in figure 9.3.

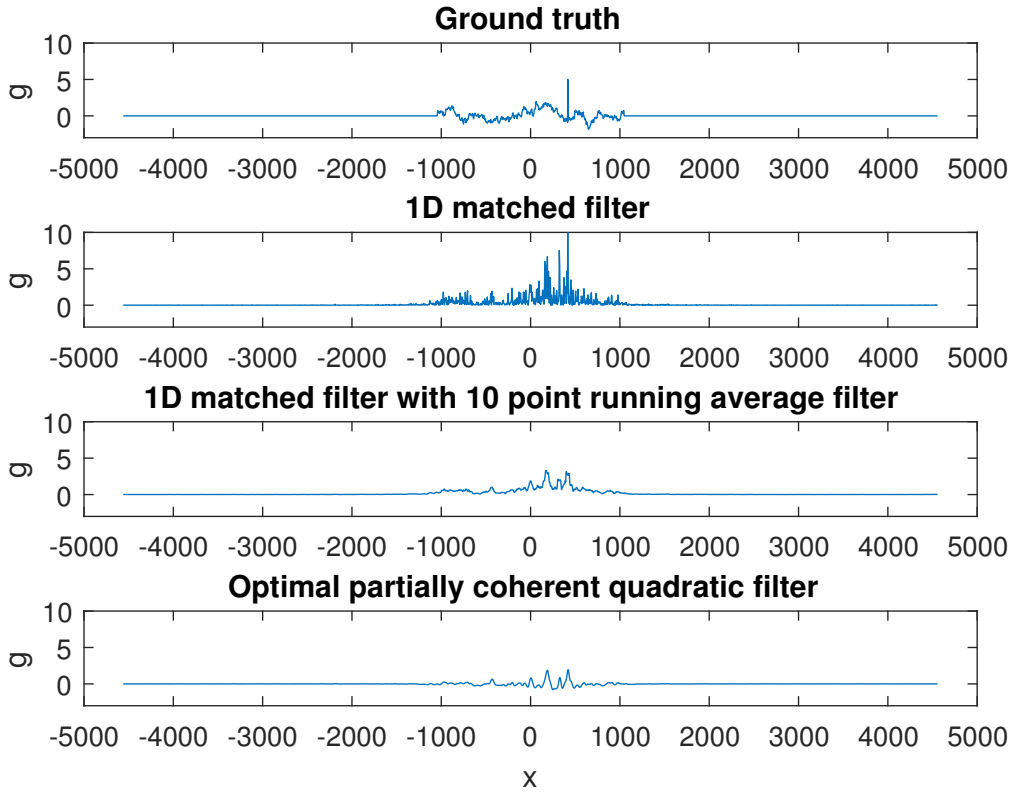

Figure 9.3: Distributed scene simulation 2. $P_r = 5$, $l_c = 208.8$ m, $\tau_{c,background} = 0.0588$ s, $\tau_{c,target} = 0.588$ s.

Keeping the power of the point target at 5, suppose that the coherence length of the background is adjusted to 2088 m, which is equal to the scene length. If the spatial coherence has any effect on the point target return it should appear in the result in figure 9.4. It may be observed that the point target remains hardly detectable, and hence the scene coherence length seems to have no significant effect.

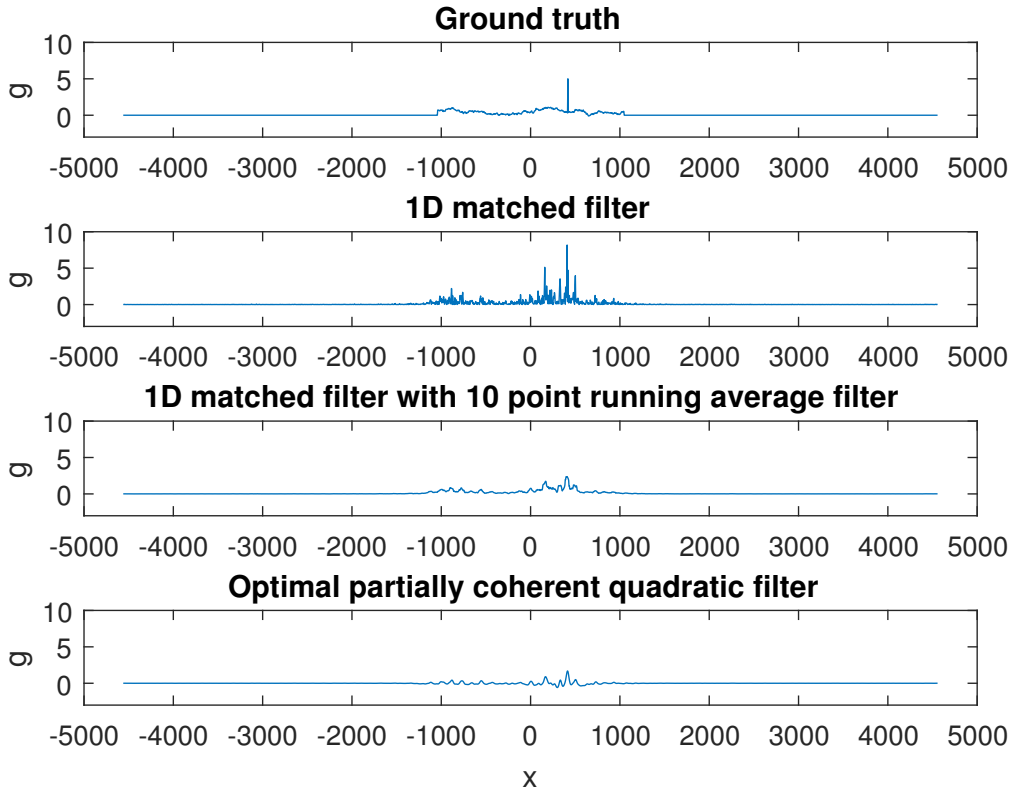

Figure 9.4: Distributed scene simulation 3. $P_r = 5$, $l_c = 2088$ m, $\tau_{c,background} = 0.0588$ s, $\tau_{c,target} = 0.588$ s.

Next the effect of reducing the coherence times of the point target and background is investigated. Let the power of the point target be restored to 10, and the scene coherence length to 208.8 m. Figure 9.5 shows the results of lowering the coherence times to $\tau_{c,background} = 0.0294$ s and $\tau_{c,target} = 0.294$ s, and figure 9.6 shows the effect of setting $\tau_{c,background} = 0.0059$ s and $\tau_{c,target} = 0.0588$ s.

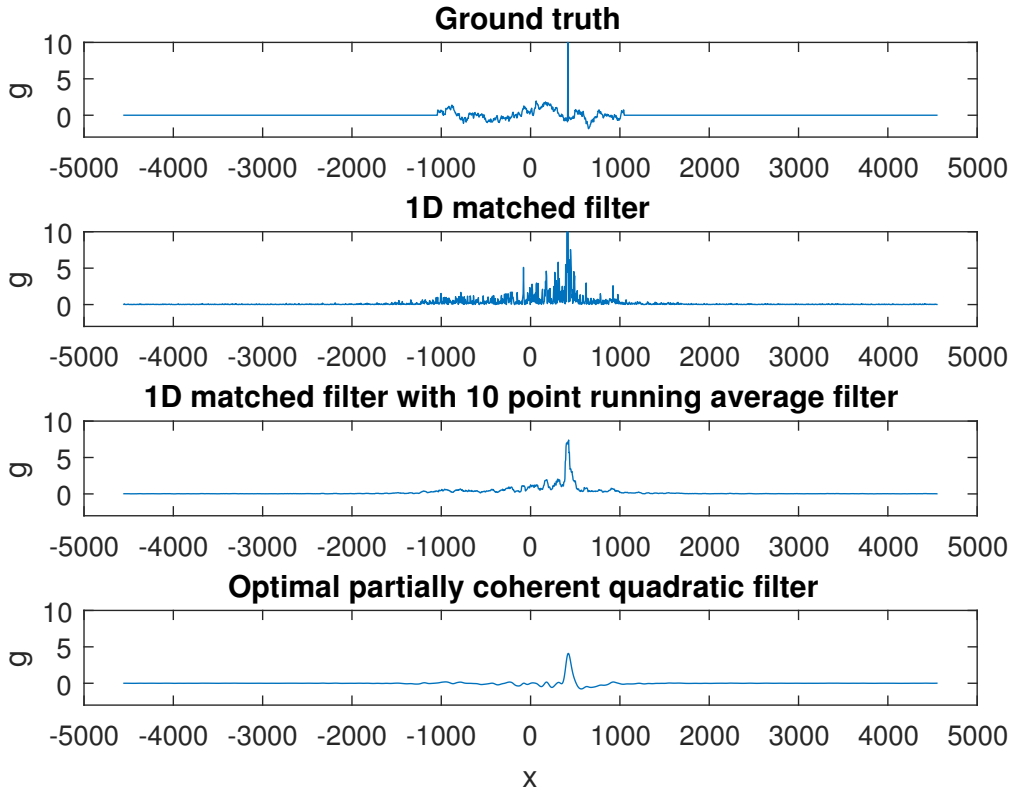

Figure 9.5: Distributed scene simulation 4. $P_r = 10$, $l_c = 208.8$ m, $\tau_{c,background} = 0.0294$ s, $\tau_{c,target} = 0.294$ s.

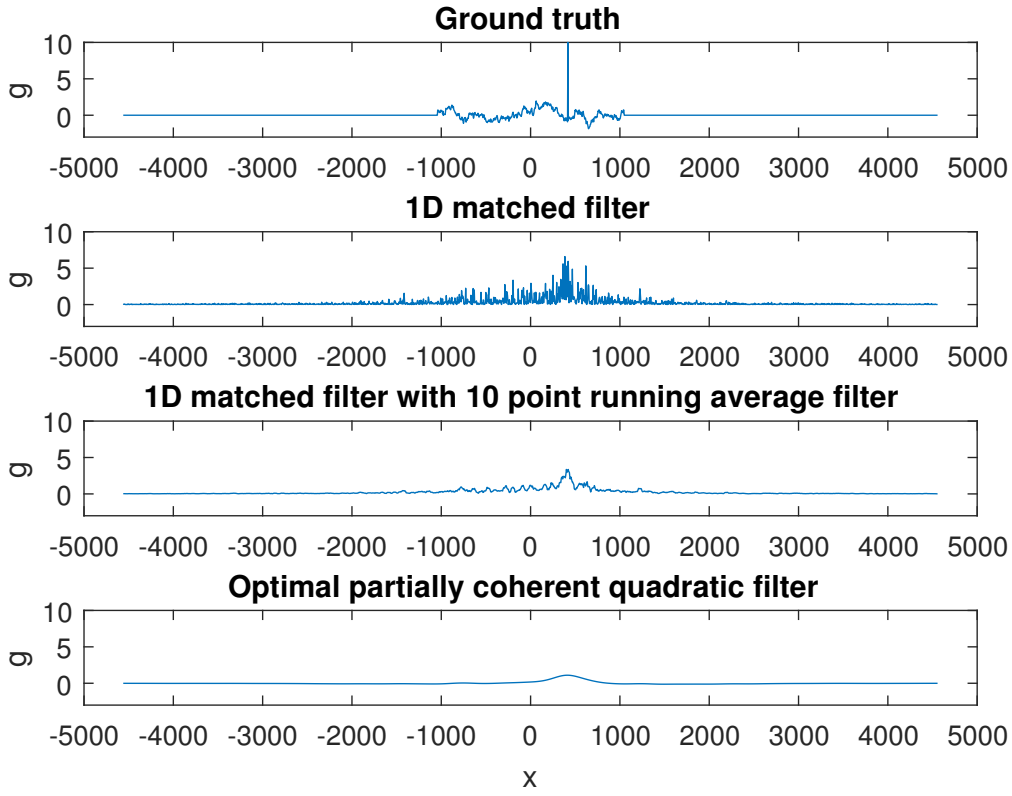

Figure 9.6: Distributed scene simulation 5. $P_r = 10$, $l_c = 208.8$ m, $\tau_{c,background} = 0.0059$ s, $\tau_{c,target} = 0.0588$ s.

As expected the return signal of the point target is weakened to the point of disappearing completely. Interestingly the 1D matched filter with a 10 point running average filter seems to perform equally well as the partially coherent quadratic filter.

9.4 Discussion

The similarity between the partially coherent quadratic filter and the 1D matched filter with a running average filter is a noteworthy result. In order to explain this, consider the expected transfer function given by equation 7.29. Recalling that:

$$\tilde{g}_\delta(\omega) = \gamma\left(\frac{\omega}{b}\right)\rho\left(\frac{\omega}{b}\right)\frac{1}{2\pi}\int \tilde{h}(\omega-\lambda)\tilde{w}(\omega-\lambda)\tilde{h}^*(-\lambda)\tilde{w}^*(-\lambda)\,d\lambda \tag{9.2}$$

is the transfer function of the quadratic filter, a closed form expression can be derived. For a complex Gaussian Fourier the transform pair is:

$$e^{-cx^2} \leftrightarrow \sqrt{\frac{\pi}{c}}e^{-\frac{\omega^2}{4c}} \tag{9.3}$$

(Smith III, 2000). Since $w(x) = e^{-cx^2}$ and $h(x) = e^{-c^*x^2}$:

$$\begin{aligned}
\tilde{h}(\omega-\lambda)\tilde{w}(\omega-\lambda)\tilde{h}^*(-\lambda)\tilde{w}^*(-\lambda) &= \sqrt{\frac{\pi}{c^*}}e^{-\frac{(\omega-\lambda)^2}{4c^*}}\cdot\sqrt{\frac{\pi}{c}}e^{-\frac{(\omega-\lambda)^2}{4c}}\cdot\sqrt{\frac{\pi}{c^*}}e^{-\frac{(-\lambda)^2}{4c^*}}\cdot\sqrt{\frac{\pi}{c}}e^{-\frac{\lambda^2}{4c}} \\
&= \frac{\pi^2}{|c|^2}e^{-\frac{(\omega-\lambda)^2}{4c}-\frac{(-\lambda)^2}{4c}}e^{-\frac{(\omega-\lambda)^2}{4c^*}-\frac{(-\lambda)^2}{4c^*}} \\
&= \frac{\pi^2}{|c|^2}e^{-\frac{\omega^2}{4c}}e^{-\frac{\lambda^2+\omega\lambda}{2c}}e^{-\frac{\omega^2}{4c^*}}e^{-\frac{\lambda^2+\omega\lambda}{2c^*}} \\
&= \frac{\pi^2}{|c|^2}e^{-\frac{\omega^2(c+c^*)}{4|c|^2}}e^{-\frac{(\lambda^2+\omega\lambda)(c+c^*)}{2|c|^2}} \\
&= \frac{4\pi^2}{a^2+b^2}e^{-\frac{a\omega^2}{a^2+b^2}}e^{-2a\frac{(\lambda^2+\omega\lambda)}{a^2+b^2}}
\end{aligned} \tag{9.4}$$

Therefore:

$$\begin{aligned}
\tilde{g}_\delta(\omega) &= \gamma\left(\frac{\omega}{b}\right)\rho\left(\frac{\omega}{b}\right)\frac{1}{2\pi}\frac{4\pi^2}{a^2+b^2}e^{-\frac{a\omega^2}{a^2+b^2}}\int e^{-2a\frac{(\lambda^2+\omega\lambda)}{a^2+b^2}}\,d\lambda \\
&= \gamma\left(\frac{\omega}{b}\right)\rho\left(\frac{\omega}{b}\right)\frac{1}{2\pi}\frac{4\pi^2}{a^2+b^2}e^{-\frac{a\omega^2}{a^2+b^2}}\sqrt{\frac{a^2+b^2}{a}}\sqrt{\frac{\pi}{2}}e^{\frac{a\omega^2}{2(a^2+b^2)}} \\
&= \gamma\left(\frac{\omega}{b}\right)\rho\left(\frac{\omega}{b}\right)\sqrt{\frac{2\pi^2}{a(a^2+b^2)}}e^{-\frac{a\omega^2}{2(a^2+b^2)}}
\end{aligned} \tag{9.5}$$

where the integral was evaluated using the `Integrate` function in Wolfram Mathematica 9.0. This is a new result which illustrates that the SAR transfer function for a quadratic filter takes the form of a Gaussian low-pass filter weighted by the autocorrelation function and the processor coherence.

Given this result it is not surprising that simply averaging the output of a 1D matched filter yields similar results.

Chapter 10

Summary and conclusions

The aim of this study was to give a well-structured introduction into Raney's formalism for partially coherent processing of SAR images, and to investigate the processing of scenes containing targets with different correlation times.

Chapter 2 covered the basis of EM radiation, which is the medium through which information is recorded by a SAR. Chapter 3 discussed some key topics in signal processing which pertain to the operation of a SAR, and chapter 4 introduced the radar as a ranging instrument. Chapter 5 thoroughly covered the principles and properties of SAR systems and introduced a simplified processing model of the azimuth channel which is the basis of Raney's quadratic filter formalism. Next the quadratic filter was introduced in chapter 6, and a filtering scheme was rederived where a non-linear system is transformed into a linear one. Concluding the theoretical part of this thesis, chapter 7 discussed the physical concept of coherence and described how a quadratic filter can represent a partially coherent SAR processor for the azimuth channel.

Finally, chapter 8 and chapter 9 presented the results of filtering simulated SAR data using a partially coherent quadratic filter. In the case of a single point target it was found that the degradation of the resolution agrees with the theoretical predictions. Furthermore a quadratic filter with a scooped envelope was tested for the purpose of processing a distributed scene where a partially coherent point target is embed-

ded in a background, the signal strength and coherence of which is significantly lower.

It was found that replacing the Gaussian envelope with the difference of two Gaussian envelopes, the latter of which is narrower than the former, produced results which were comparable to processing the data with a standard matched filter and applying a running average filter. This correspondence was explained by examining the expected transfer function of the SAR system including the prefilter. An explicit form of the transfer function was derived, and it was found to be the product of the processor envelope, the scene autocorrelation function, and a Gaussian function. The whole system therefore acts as a low-pass filter[1] for this particular choice of quadratic filter, which explains why averaging the output of a matched filter processor produces similar results.

It may therefore be concluded that the partially coherent quadratic filters considered here, under the he criterion of maximizing the ratio (expected signal)^2/(noise variance), do not offer any significant potential for target detection compared to standard SAR processing.

Future work on this topic might consider other forms of quadratic filters by varying the choice of the quadratic filter envelope γ. This will necessarily include ascertaining which functions are permissible due to the requirements posed on partially coherent quadratic filters by Raney, and whether or not it is possible to relax these requirements, one example of which has been presented in this thesis. The existence of the Fourier transform of partially coherent quadratic filters for different choices of γ should then be thoroughly investigated.

Furthermore, the formalism in itself is interesting and may have applications not considered in this study. The presentation of Raney's work on this topic is therefore considered part of the contribution of this thesis, in the hope that it may prove useful

[1]The scooped quadratic filter might also qualify as a band-pass filter. However, the filter is still band-limited by the target autocorrelation function $e^{-\frac{A_{target}}{2}u^2}$ in equation 9.1.

for other purposes.

Bibliography

Alaska Satellite Facility. (n.d.). *Seasat satellite's synthetic aperture radar: History & tech specs.* Retrieved 28.02.2018, from `https://www.asf.alaska.edu/seasat/about/`

Alpers, W., & Rufenach, C. (1979). The effect of orbital motions on synthetic aperture radar imagery of ocean waves. *IEEE Transactions on Antennas and Propagation*, *27*(5), 685-690. doi: 10.1109/TAP.1979.1142163

Anton, H., & Rorres, C. (2011). *Elementary linear algebra with supplemental applications* (10th ed.). John Wiley and Sons, Inc.

Barile, M. (n.d.). *Hermitian form.* Retrieved 15.02.2018, from `http://mathworld.wolfram.com/HermitianForm.html`

Beal, R. C., Tilley, D. G., & Monaldo, F. M. (1983). Large- and small-scale spatial evolution of sigitally processed ocean wave spectra from SEASAT synthetic sperture sadar. *Journal of Geophysical Research*, *88*(C3), 1761-1778.

Beran, M. J., & Parrent, G. B. (1963). *Theory of partial coherence.* Englewood Cliffs , N. J.: Prentice Hall, Inc.

Brown, W. M. (1963). *Analysis of linear time-invariant systems.* McGraw-Hill Book Company, Inc.

Carande, R. E. (1994). Estimating ocean coherence time using dual-baseline interferometric synthetic aperture radar. *IEEE Transaction on Geoscience and Remote Sensing*, *34*(2), 846-854. doi: 10.1109/36.298012

Cumming, I. G., & Wong, F. H. (2005). *Digital processing of synthetic aperture radar data: algorithms and implementation.* Artech House.

Deserno, M. (2002). *How to generate exponentially correlated gaussian random numbers.* Retrieved 31.03.2018, from `https://www.cmu.edu/biolphys/deserno/pdf/corr_gaussian_random.pdf`

Elachi, C., & van Zyl, J. (2006). *Introduction to the physics and techniques of remote sensing.* Wiley-Interscience.

Feynman, R., Leighton, R. B., & Sands, M. (1963). *The Feynman lectures on physics* (Vol. 1). Addison Wesley Publishing Company.

Galati, G. (2016). *100 years of radar.* Springer. doi: 10.1007/978-3-319-00584-3

Gonzales, R. E., & Woods, R. E. (2010). *Digital image processing* (3rd ed.). Upper Saddle River, NJ: Pearson Education, Inc.

Griffiths, D. J. (2013). *Introduction to electrodynamics* (4th ed.). Upper Saddle River, NJ: Pearson Education, Inc.

Harger, R. O. (1970). *Synthetic aperture radar: theory and design.* New York: Academic Press.

Jenkins, F. A., & White, H. E. (1957). *Fundamentals of optics* (3rd ed.). McGraw-Hill Book Company, Inc.

Jet Propulsion Laboratory. (2001). *20 years of shuttle imaging radar.* Retrieved 28.02.2018, from `https://www.jpl.nasa.gov/news/news.php?feature=422`

Kasilingam, D. P., & Shemdin, O. H. (1990). Models for synthetic aperture radar imaging of the ocean' a comparison. *Journal of Geophysical Research*, *95*(C9), 16263-16276.

Kingsley, S., & Quegan, S. (1992). *Understanding radar systems.* McGraw-Hill Book Company, Inc.

Massonet, D., & Souyris, J.-C. (2008). *Imaging with synthetic aperture radar*. EPFL Press.

MathWorks. (n.d.). *conv*. Retrieved 23.04.2018, from `https://se.mathworks.com/help/matlab/ref/conv.html`

McClellan, J. H., Schafer, R. W., & Yoder, M. A. (2003). *Signal prcessing first*. Upper Saddle River: Pearson Prentice Hall.

Norris, P. (2008). *Spies in the sky: Surveillance satellites in war and peace*. Chichester: Praxis Publishing, Ltd.

Oliver, C., & Quegan, S. (2004). *Understanding synthetic aperture radar images*. Raleigh, NC: Scitech Publishing, Inc.

Raney, R. K. (1969a). Quadratic filter theory and partially coherent optical systems. *Journal of the Optical Society of America*, *59*(9), 1149-1154.

Raney, R. K. (1969b). *Theory of quadratic filters* (Unpublished doctoral dissertation). University of Michigan, Ann Arbor.

Raney, R. K. (1971). Synthetic aperture radar imaging and moving targets. *IEEE Transactions on Aerospace and Electronic Systems*, *AES-7*(3). doi: 10.1109/TAES.1971.310292

Raney, R. K. (1980a). Sar processing of partially coherent phenomena. *Int. J. Remote Sensing*, *1*(1), 29-51.

Raney, R. K. (1980b). SAR response to partially coherent phenomena. *IEEE Transactions on Antennas and Propagation*, *AP-28*(6), 777-787. doi: 10.1109/TAP.1980.1142446

Raney, R. K. (1981a). Transfer functions for partially coherent SAR systems. *IEEE Transactions on Aerospace and Electronic Systems*, *AES-19*(5), 740-750. doi: 10.1109/TAES.1983.309375

Raney, R. K. (1981b). Wave orbital velocity, fade, and sar response to azimuth waves. *IEEE Journal of Oceanic Engineering*, *6*(4), 140-146. doi: 10.1109/JOE .1981.1145495

Shemer, L., & Marom, M. (1993). Estimates of ocean coherence time by an interferometric SAR. *Int. J. Remote Sensing*, *14*(16), 3021-3029.

Smith III, J. O. (2000). *Fourier transform of complex Gaussian.* Retrieved 31.03.2018, from `https://www.dsprelated.com/freebooks/sasp/Fourier_Transform_Complex_Gaussian.html`

Stutzman, W. L., & Thiele, G. A. (2013). *Antenna theory and design* (3rd ed.). John Wiley & Sons, Inc.

The Optical Society. (2005). *In memoriam: Emmett leith.* Retrieved 28.02.2018, from `https://www.osa.org/en-us/about_osa/newsroom/obituaries/earlier/leith/`

Vachon, P. W. (1983). *Synthetic aperture radar imaging of the ocean surface: theoretical considerations, and experiments with simulated and actual SAR imagery* (Doctoral dissertation, The University of British Columbia). doi: 10.14288/1.0053106

Weisstein, E. W. (n.d.). *Spherical coordinates.* Retrieved 13.02.2018, from `http://mathworld.wolfram.com/SphericalCoordinates.html`

Zauderer, E. (2006). *Partial differential equations of applied mathematics* (3rd ed.). Hoboken, New Jersey: John Wiley & Sons, Inc.

Zernike, F. (1938). The concept of degree of coherence and its application to optical problems. *Physika*, *5*(8), 785-795. doi: 10.1016/S0031-8914(38)80203-2

Appendices

Appendix A

Derivation of the half power beamwidth

The power of the electric field is proportional to the square of the amplitude, and at $\theta = 0$ there is no contribution from the phase factor. Therefore, in the ratio $\frac{E^2(\beta)}{E^2(0)}$ all constants cancel, and the half power beam width β is obtained through equation 4.15:

$$\left(\frac{\sin\left(\frac{kD\sin\frac{\beta}{2}}{2}\right)}{\frac{kD\sin\frac{\beta}{2}}{2}} \right)^2 \equiv \mathrm{sinc}^2\left(\frac{kD\sin\frac{\beta}{2}}{2}\right) = \frac{1}{2} \tag{A.1}$$

which, according to Elachi and van Zyl (2006) can be solved numerically to yield:

$$\beta = 0.88\frac{\lambda}{D} \tag{A.2}$$

However, setting $D = \lambda = 1$ in the integral and solving using the Mathematica function `FindRoot`, the answer comes out as 0.918.

Following Stutzman and Thiele (2013, p. 130), the equation:

$$\mathrm{sinc}\, x = \frac{1}{\sqrt{2}} \tag{A.3}$$

can be solved the same way to obtain $x \approx \pm 1.392$. Using this to solve for β:

$$\begin{aligned} \frac{1}{2}kD\sin\frac{\beta}{2} &= 1.392 \\ \implies \beta &= 2\arcsin\frac{2.784}{kD} \\ &= 2\arcsin\frac{2.784\lambda}{2\pi D} \\ &\approx 2\arcsin 0.4431\frac{\lambda}{D} \end{aligned} \tag{A.4}$$

If $\frac{\lambda}{D} \ll 1$, then the arcsin can be Taylor expanded to first order in $\frac{\lambda}{D}$ around 0. The first order Taylor expansion of $\arcsin x$ is equal to x, and therefore:

$$\beta \approx 0.886\frac{\lambda}{D} \tag{A.5}$$

which is close, but not quite. If equation A.1 is expressed in decibel and solved for the value of β at which the difference is -3 dB:

$$10\log_{10}\operatorname{sinc}\left(\frac{kD\sin\frac{\beta}{2}}{2}\right) = -3dB \tag{A.6}$$

then β is the angle at which the power drops off by a factor $10^{\frac{-3dB}{10}} \approx 0.5011$ and the same procedure as above does indeed yield the approximation:

$$\beta \approx 0.884\frac{\lambda}{D} \tag{A.7}$$

In either case the constant factor is approximately equal to 1.

Appendix B

Derivation of the SAR transfer function

The transfer function of a partially coherent SAR system is here rederived following Raney (1981b).

The expected impulse response of a partially coherent SAR system is given by:

$$\begin{aligned} E[g_\delta(u)] &= E\left[\iint Q(u-x,u-y)w(x)w^*(y)\alpha(x|0)\alpha^*(y|0)\,dx\,dy\right] \\ &= \iint Q(u-x,u-y)w(x)w^*(y)E\left[\alpha(x|0)\alpha^*(y|0)\right]\,dx\,dy \\ &= \iint Q(u-x,u-y)w(x)w^*(y)\rho(y-x)\,dx\,dy \end{aligned} \tag{B.1}$$

assuming that $\{\alpha\}$ has an autocorrelation function ρ (Raney, 1980b, p. 779).

Augmenting variables:

$$G_\delta(u) = \iint Q(u-x,v-y)w(x)w^*(y)\rho(y-x)\,dx\,dy \tag{B.2}$$

Define:

$$Q_w(x,y) = w(x)w^*(y)\rho(y-x) \tag{B.3}$$

such that $G_\delta(u)$ can be written as:

$$G_\delta(u) = \iint Q(u-x, v-y) Q_w(x,y)\, dx\, dy \tag{B.4}$$

Raney (1981a, p. 743) states that $Q_w(x,y)$ satisfies the requirements of a quadratic filter. Taking the Fourier transform of $G_\delta(u)$ yields:

$$\tilde{G}_\delta(u) = \tilde{Q}(\omega,\lambda)\tilde{Q}_w(\omega,\lambda) \equiv \tilde{Q}_T(\omega,\lambda) \tag{B.5}$$

Next, Raney (1981b) applies the principle of stationary phase, whereby the integral over a function:

$$f(t) = f_a(t) e^{i\varphi(t)} \tag{B.6}$$

can be written as:

$$\int f(t)\, dt = \frac{\sqrt{2\pi} f_a(t^*)}{\sqrt{|\varphi''(t^*)|}} \tag{B.7}$$

where $\cdot^*$ does not denote complex conjugation, but t^* is the point at which $\varphi'(t) = 0$. This approximation is valid under the assumption of large TBP. Applying this to the quadratic filters in equation B.5 yields:

$$\begin{aligned} \tilde{Q}(\omega,\lambda) &= \gamma\left(\frac{\lambda+\omega}{b}\right)\tilde{h}(\omega)\tilde{h}^*(-\lambda) \\ \tilde{Q}_w(\omega,\lambda) &= \rho\left(\frac{\lambda+\omega}{b}\right)\tilde{h}(\omega)\tilde{h}^*(-\lambda) \end{aligned} \tag{B.8}$$

(Raney, 1981b, p. 749). Therefore:

$$\tilde{Q}_T(\omega,\lambda) = \gamma\left(\frac{\lambda+\omega}{b}\right)\rho\left(\frac{\lambda+\omega}{b}\right)\tilde{h}(\omega)\tilde{h}^*(-\lambda)\tilde{w}(\omega)\tilde{w}^*(-\lambda) \tag{B.9}$$

Finally, applying association of variables:

$$\begin{aligned} \tilde{g}_\delta(\omega) &= \frac{1}{2\pi}\int \tilde{Q}_T(\omega-\lambda,\lambda)\, d\lambda \\ &= \gamma\left(\frac{\omega}{b}\right)\rho\left(\frac{\omega}{b}\right)\frac{1}{2\pi}\int \tilde{h}(\omega-\lambda)\tilde{w}(\omega-\lambda)\tilde{h}^*(-\lambda)\tilde{w}^*(-\lambda)\, d\lambda \end{aligned} \tag{B.10}$$

Appendix C

Source code

C.1 Main scripts

C.1.1 Linear filter demo with point target

```
clear all;
close all;

% Set seed
rng(5705)

% Radar parameters (Cumming & Wong, 2003, table 4.1)
R = 800e3;          % Radar altitude (m)
V = 7100;           % Effective radar velocity (m/s)
lambda = 0.057;     % Radar wavelength (m)
L = 10;             % Antenna length (m)
PRF = 1700;         % Azimuth sampling rate/PRF (Hz)
beta = lambda/L;    % Beamwidth
Ts = 1/PRF;         % Sampling period

% Filter energy
```

```
load('E.mat'); % Constant equal to 4.8003e+05

% Point target
f = 1;

% Noise sd
sigma_n = 0.25;

% Coherence time
tau_c = 0.01;

% Raney parameters
a = 2*pi/(R*beta)^2;
b = 4*pi/(lambda*R);
c = a/2 + 1i*b/2;

% Time vector. Target enters beamwidth at t0 and is directly beneath the
% radar platform at t=0.
t0 = R*tan(beta)/V;
t = -t0:Ts:t0-Ts;

% Azimuth prefilter
w = exp(-c*(V*t).^2);
L_w = length(w);

% Convolve target function with azimuth prefilter
% Assume that the scene has zero reflectivity around f(t),
% so that the full convolution is kept.
fw = conv(f,w);
L_fw = length(fw);
```

```
% Generate Gaussian noise with standard deviation sigma_n
n = sigma_n*(randn(1,L_fw) + 1i*randn(1,L_fw));

% Number of lags over which the target is coherent
numlags = tau_c/Ts;

% Phase error vector
theta = mycorrgn(L_fw, numlags);
alpha = exp(1i*pi*theta);

% Apply phase errors
fw = fw.*alpha;

% Matched filter
h = conj(w);

% Apply matched filter, throw away zero-padded parts
fwh = conv(fw + n, h,'same');

% Magnitude squared
g = abs(fwh).^2;

% Normalize by the enregy of the filter
g = g/E;

% Output time vector
eta = -length(g)/2*Ts:Ts:(length(g)/2-1)*Ts;

% Plot output
figure(1)
plot(V*eta,g)
```

```
ylim([0,1])
xlabel('x','fontsize',11)
ylabel('g','fontsize',11)
```

C.1.2 Quadratic filter demo with point target

```
clear all;
close all;

% Set seed
rng(5705)

% Filter energy
load('E.mat'); % Constant equal to 4.8003e+05

% Radar parameters (Cumming & Wong, 2003, table 4.1)
R = 800e3;          % Radar altitude (m)
V = 7100;           % Effective radar velocity (m/s)
lambda = 0.057;     % Radar wavelength (m)
L = 10;             % Antenna length (m)
PRF = 1700;         % Azimuth sampling rate/PRF (Hz)
beta = lambda/L;    % Beamwidth
Ts = 1/PRF;         % Sampling period

% Noise sd
sigma_n = 0.25;

% Coherence time
tau_c = 0.01;

% Raney parameters
```

```
a = 2*pi/(R*beta)^2;
b = 4*pi/(lambda*R);
c = a/2 + 1i*b/2;

% Target
f = 1;

% Time vector. Target enters beamwidth at -t0 and is directly beneath the
% radar platform at t=0.
t0 = R*tan(beta)/V;
t = -t0:Ts:t0;

% Azimuth prefilter
w = exp(-c*(V*t).^2);
L_w = length(w);

% Convolve target function with azimuth prefilter
% Assume that the scene has zero reflectivity around f(t),
% so that the full convolution is kept.
fw = conv(f,w);
L_fw = length(fw);

% Generate Gaussian noise with standard deviation sigma_n
n = sigma_n*(randn(1,L_fw) + 1i*randn(1,L_fw));

% Number of lags over which the target is coherent
numlags = tau_c/Ts;

% Phase error vector
alpha = exp(1i*pi*mycorrgn(L_fw, numlags));
```

```
% Apply phase errors
fw = fw.*alpha;

% Coherence parameters
B = 2/(tau_c/10*V)^2;
A = 0;

% Quadratic filter
x = V*t;
y = x;
[Y,X] = meshgrid(x,y);
Q = exp(-(Y-X).^2*A/2) .* exp(-X.^2*conj(c)) .* exp(-Y.^2*c);
N_Q = size(Q,1);

% Target image
W = transpose(fw+n)*conj(fw+n);

% Zero padding
n_pad = 2*size(W);
Q_pad = padarray(Q,n_pad-size(Q),'post');
W_pad = padarray(W,n_pad-size(W),'post');

% Convolution
G = fft2(Q_pad) .* fft2(W_pad);
G_inv = ifft2(G);

% Remove zero padding
G_inv_cropped = G_inv(1:L_fw + N_Q - 1, 1:L_fw + N_Q - 1);
G_inv_cropped_diag = transpose(diag(G_inv_cropped));
g_full = real(G_inv_cropped_diag)/E;
```

```
% Crop output vector
if mod(L_fw,2) == 0
    g = g_full((L_fw)/2:length(g_full)-(L_fw)/2);
else
    g = g_full((L_fw-1)/2:length(g_full)-(L_fw-1)/2-1);
end

% Time vector
eta = -length(g)/2*Ts:Ts:(length(g)/2-1)*Ts;

% Plot output
figure(2)
plot(V*eta,g)
ylim([0,1])
xlabel('x','fontsize',11)
ylabel('g','fontsize',11)
```

C.1.3 Quadratic filter demo with distributed scene

```
clear all;
close all;

% Set seed
rng(5705);

% Filter energy
load('E.mat'); % Constant equal to 4.8003e+05

% Radar parameters (Cumming & Wong, 2003, table 4.1)
R = 800e3;          % Radar altitude (m)
V = 7100;           % Effective radar velocity (m/s)
```

```
lambda = 0.057;     % Radar wavelength (m)
L = 10;             % Antenna length (m)
PRF = 1700;         % Azimuth sampling rate/PRF (Hz)
beta = lambda/L;    % Beamwidth
Ts = 1/PRF;         % Sampling period

% Raney parameters
a = 2*pi/(R*beta)^2;
b = 4*pi/(lambda*R);
c = a/2 + 1i*b/2;

% Generate scene
SL = 500;
tpos = 100;
Pr = 10;
numlags1 = 50;
numlags2 = 100;
numlags3 = 1000;

[f,fw] = generate_scene(SL, tpos, Pr, numlags1, numlags2, numlags3);
L_fw = length(fw);
L_f = length(f);

sigma_n = 0.25*Pr;

% Time vector. Target enters beamwidth at -t0 and is directly beneath the
% radar platform at t=0.
t0 = R*tan(beta)/V;
t = -t0:Ts:t0;

% Linear filter
```

```
w = exp(-c*(V*t).^2);
h = conj(w);
L_w = length(w);

% Generate Gaussian noise with standard deviation sigma_n
n = sigma_n*(randn(1,L_fw) + 1i*randn(1,L_fw));

% Linear filter
g1 = abs(conv(h,fw+n,'same')).^2/E;

% Quadratic filter
A = 2/(numlags2/10*Ts*V)^2;
B = 2/(numlags3/10*Ts*V)^2;
x = V*t;
[Y,X] = meshgrid(x,x);
Q = (exp(-(Y-X).^2*B/2) - exp(-(Y-X).^2*A/2)) .* ...
    exp(-X.^2*conj(c)) .* exp(-Y.^2*c);
N_Q = size(Q,1);

% Target image
W = transpose(fw+n)*conj(fw+n);

% Zero padding
n_pad = 2*size(W);
Q_pad = padarray(Q,n_pad-size(Q),'post');
W_pad = padarray(W,n_pad-size(W),'post');

% Convolution
G = fft2(Q_pad) .* fft2(W_pad);
G_inv = ifft2(G);
```

```
% Remove zero padding
G_inv_cropped = G_inv(1:L_fw + N_Q - 1, 1:L_fw + N_Q - 1);
G_inv_cropped_diag = transpose(diag(G_inv_cropped));
g2_full = real(G_inv_cropped_diag)/E;

% Crop vectors
if mod(L_fw,2) ~= 0
    g2 = g2_full((L_fw-1)/2:length(g2_full)-(L_fw-1)/2-1);
    f_cropped = f((L_fw-1)/2:length(g2_full)-(L_fw-1)/2-1);
else
    g2 = g2_full((L_fw)/2:length(g2_full)-(L_fw)/2);
    f_cropped = f((L_fw)/2:length(g2_full)-(L_fw)/2);
end

% Time vector
eta = -length(g1)/2*Ts:Ts:(length(g1)/2-1)*Ts;

ylimits = [-3,10];

% n-point sliding averaging filter
nfilt = 10;

% Plot output
figure(3)
subplot(4,1,1)
plot(V*eta,f_cropped)
title('Ground truth','fontsize',11)
ylabel('g')
ylim(ylimits)
subplot(4,1,2)
plot(V*eta,g1)
```

```
title('1D matched filter','fontsize',11)
ylabel('g')
ylim(ylimits)
subplot(4,1,3)
plot(V*eta,conv(g1,ones(1,nfilt)/nfilt,'same'))
title('1D matched filter with 10 point running average filter','fontsize',11)
ylabel('g')
ylim(ylimits)
subplot(4,1,4)
plot(V*eta,g2)
title('Optimal partially coherent quadratic filter','fontsize',11)
ylabel('g')
ylim(ylimits)
xlabel('x')
```

C.2 Functions

C.2.1 mycorrgn

```
function [r] = mycorrgn(L, tau)
%MYCORRGN Generate correlated Gaussian random vector
%   Creates a Gaussian random vector with a given coherence time
%
%   See https://www.cmu.edu/biolphys/deserno/pdf/corr_gaussian_random.pdf
%   for details.
%
%   L:      Length of output vector
%   tau:    Number of lags over which the output vector is coherent

g = randn(1,L);
r = zeros(1,L);
```

```
f = exp(-1/tau);

r(1) = g(1);

for n=1:L-1
    r(n+1) = f*r(n) + sqrt(1-f^2)*g(n+1);
end

end
```

C.2.2 generate_scene

```
function [f,fw] = generate_scene(SL,tpos,Pr,numlags1,numlags2,numlags3)
%GENERATE_SCENE Generate a simulated SAR scene
%   Creates a simulated range gate with targets and background,
%   both of which have a given coherence time.
%   A spatial coherence is also applied.
%
%   SL:         number of elements in scene vector
%   tpos:       target positions
%   Pr:         target power
%   numlags1:   number of spatial lags over which the background is
%               coherent
%   numlags2:   number of temporal lags over which the background is
%               coherent
%   numlags3:   number of temporal lags over which the target is coherent

% Radar parameters (Cumming & Wong, 2003, table 4.1)
R = 800e3;          % Radar altitude (m)
V = 7100;           % Effective radar velocity (m/s)
lambda = 0.057;     % Radar wavelength (m)
```

```
L = 10;              % Antenna length (m)
PRF = 1700;          % Azimuth sampling rate/PRF (Hz)
beta = lambda/L;     % Beamwidth
Ts = 1/PRF;          % Sampling period

% Raney parameters
a = 2*pi/(R*beta)^2;
b = 4*pi/(lambda*R);
c = a/2 + 1i*b/2;

% Time vector. Target enters beamwidth at -t0 and is directly beneath the
% radar platform at t=0.
t0 = R*tan(beta)/V;
t = -t0:Ts:t0;
L_t = length(t);

% Azimuth prefilter
w = exp(-c*(V*t).^2);

% Generate target vector
f = mycorrgn(SL,numlags1);
tpos = SL/2 + tpos;

% Target positions
for i=1:length(tpos)
    f(tpos(i)) = Pr;
end

% Zero padding
f = padarray(f,[0,L_t-1],'both');
```

```
% Preallocation
L_fw = SL + L_t - 1;
fw = zeros(1,L_fw);
theta = zeros(L_fw,SL);

% Correlation matrix
for j=1:SL % Background
    theta(:,j) = mycorrgn(L_fw,numlags2);
end

for i=1:length(tpos) % Targets
    theta(:,tpos(i)) = mycorrgn(L_fw,numlags3);
end

% zero padding
theta = padarray(theta,[0,L_t-1],'both');

% Convolution
for i=1:L_fw
    f_sub = f(i:i+L_t-1);
    theta_sub = theta(i,i:i+L_t-1);
    fw(i) = sum(fliplr(w).*f_sub.*exp(1i*pi*theta_sub));
end

end
```